3-D SAM

Seconda parte

organization of mixed - monolayers

3D SAMs composed of thiols with immiscible chains

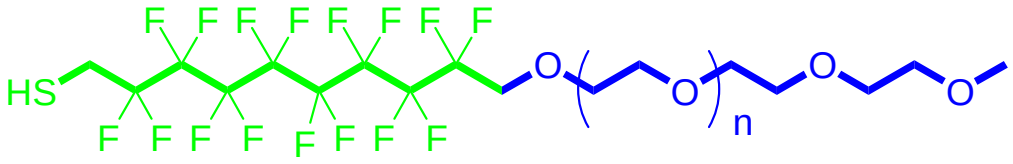

n = 8,9

HS-F8-PEG

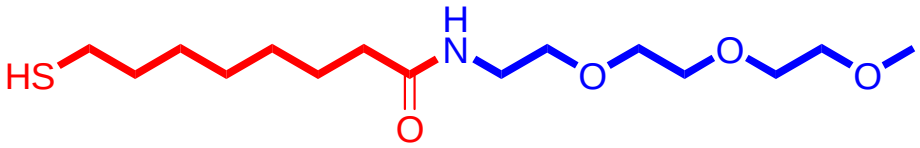

HS-C8-TEG

ESR Spectroscopy as a tool to investigate the monolayer properties

phase segregation of hydrogenated/fluorinated units

block terpolymer

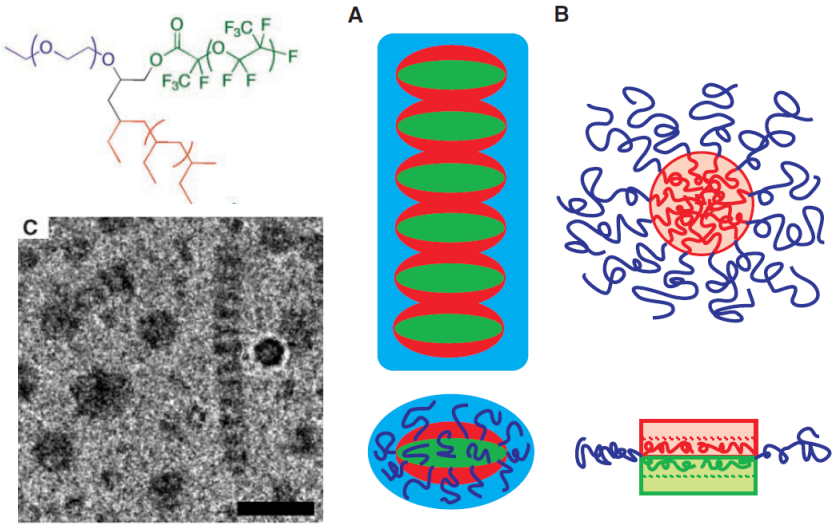

T. P. Lodge et al. *Science* **2004**, *306*, 98

monolayers

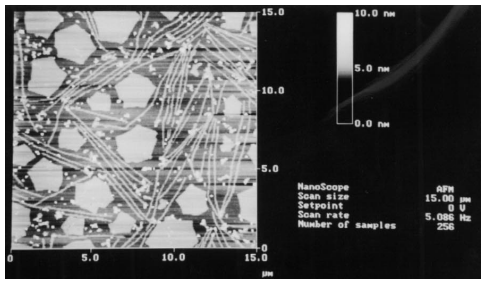

AFM images of a mixed monolayer of 1:1 $C_{18}H_{37}SO_3Na$–$C_8F_{17}COOH$ deposited on a freshly cleaved mica surface at a compression rate of 35 cm^2 min^{-1}. *Coll. Surf. A*, **1999**, *157*, 63–71.

Liposomes

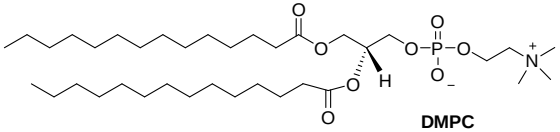

DMPC

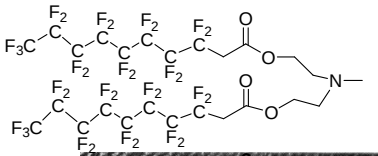

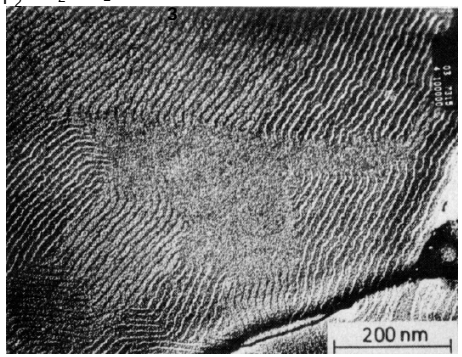

Freeze fracture electron micrograph of a phase-separated liposomal membrane (95 mol % **DMPC** and 5 mol % fluorinated lipid **3**. The ripple structure shows the parts of membrane composed of DMPC, surrounding a domain of the fluorinated lipid (smooth surface). R. Elbert, T. Folda, and H. Ringsdorf *J. Am. Chem. Soc.* **1984**, *106*, 7687-1692

metal nanoparticles protected by fluorinated ligands

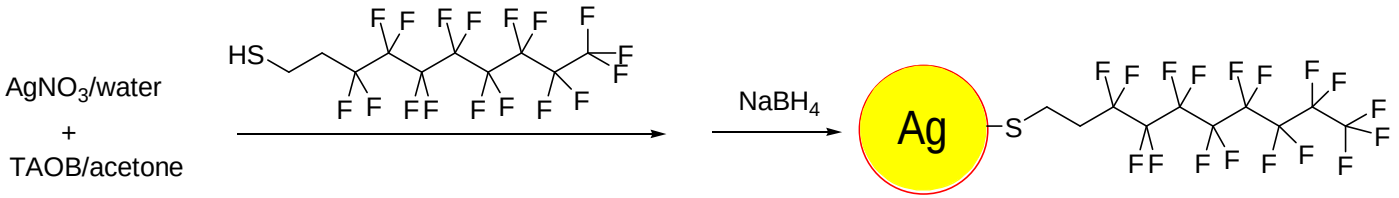

K. P. Johnston, B. A. Korgel et al. *JACS* **2000**, *122*, 4245.

dispersion in acetone and liquid and sc. CO_2

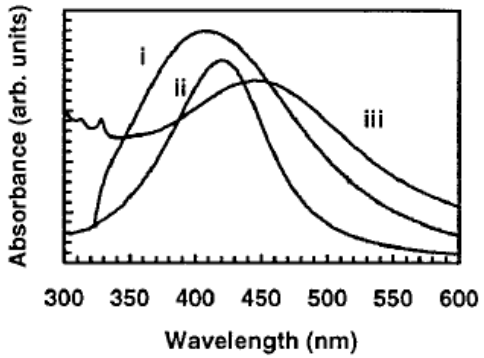

UV-visible absorbance spectra of AgNPs (i) coated with fluorinated ligands dispersed in acetone; (ii) coated with hydrocarbon ligands dispersed in hexane; (iii) coated with fluorinated ligands dispersed in sc-CO_2.

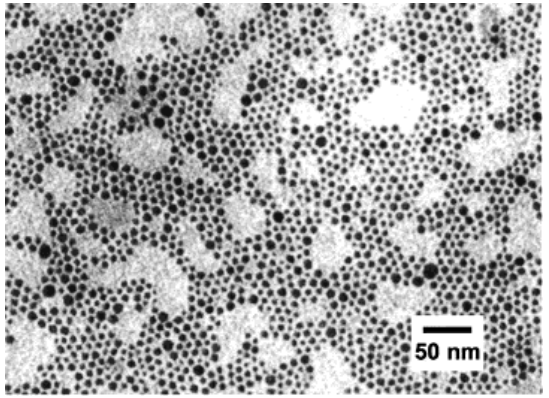

TEM image of silver nanocrystals coated with fluorinated ligands.

average size 5.5 nm

gold nanoparticles protected by fluorinated ligands

- use of commercially available *F*-thiols

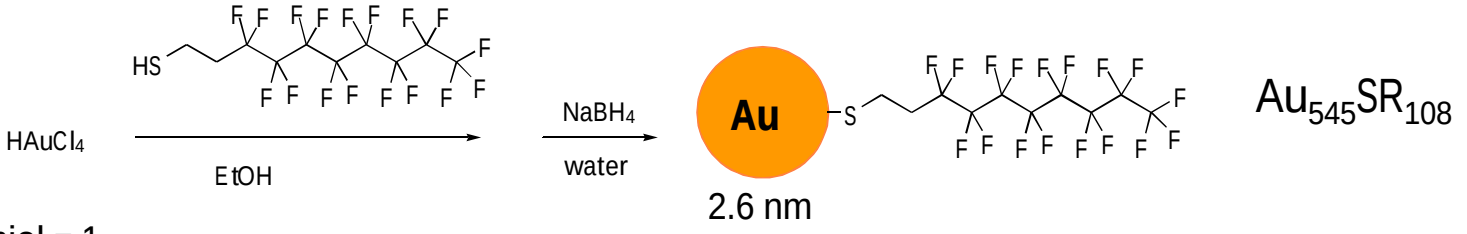

$Au_{545}SR_{108}$

Au / thiol = 1

T. Yonezawa, et al. *Langmuir*, **2001**, *17*, 2291-2293.

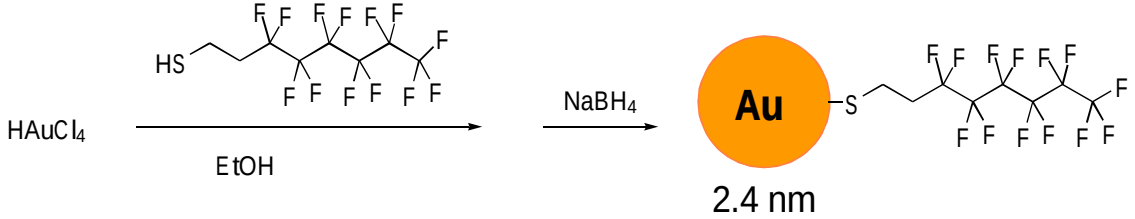

insoluble in common organic solvents:
ethanol, acetone, chloroform, DMSO

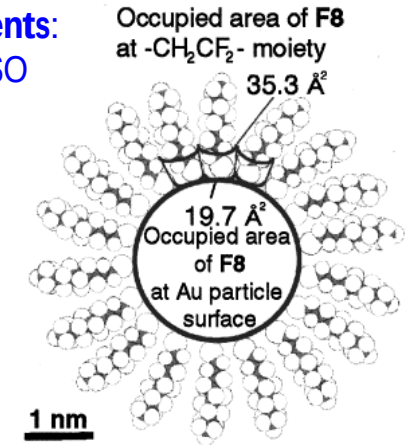

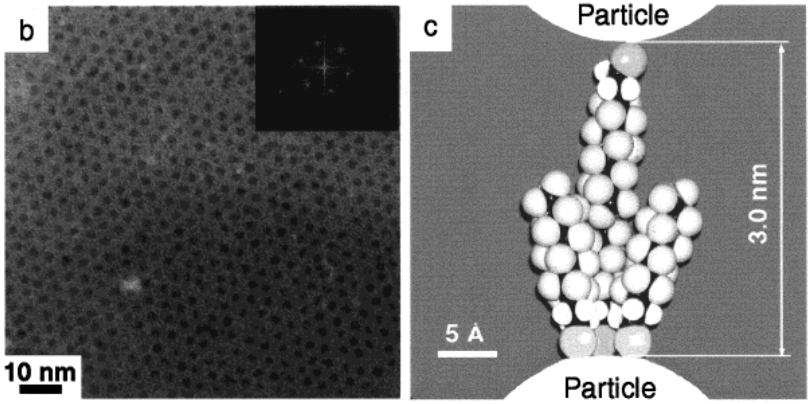

a dispersion in HCFC-225 dropcasted on a carbon-coated copper grid displays ordered hexagonal assembly

gold nanoparticles protected by fluorinated ligands

- synthesis by ligand exchange

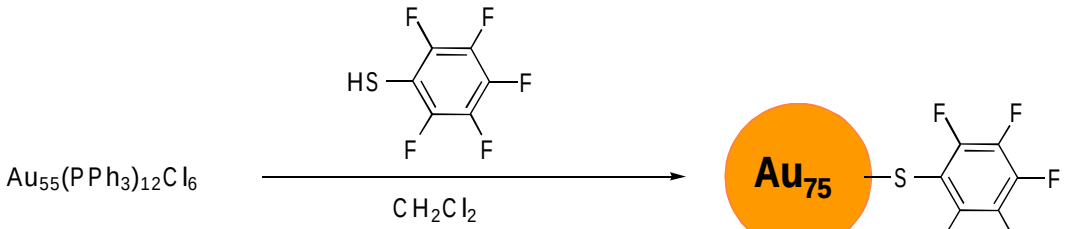

~ 1.4 nm

soluble in CH_2Cl_2, THF, DMF

- synthesis by Brust reaction

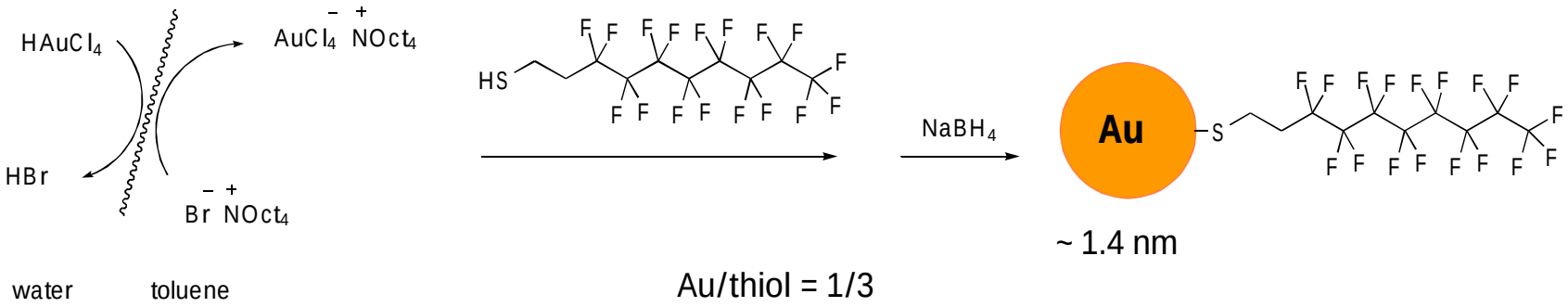

~ 1.4 nm

Au/thiol = 1/3

AuNPs soluble in non polar fluorinated solvents only

A. Dass, R. Guo, J. B. Tracy, R. Balasubramanian, A. D. Douglas, R. W. Murray *Langmuir*, **2008**, *24*, 310-315.

- Au/thiol = 3/1 averge core diameter 2.5 nm; J. Im, A. Chandekar, J. E. Whitten *Langmuir*, **2009**, *25*, 4288-4292.

gold nanoparticles protected by fluorinated ligands

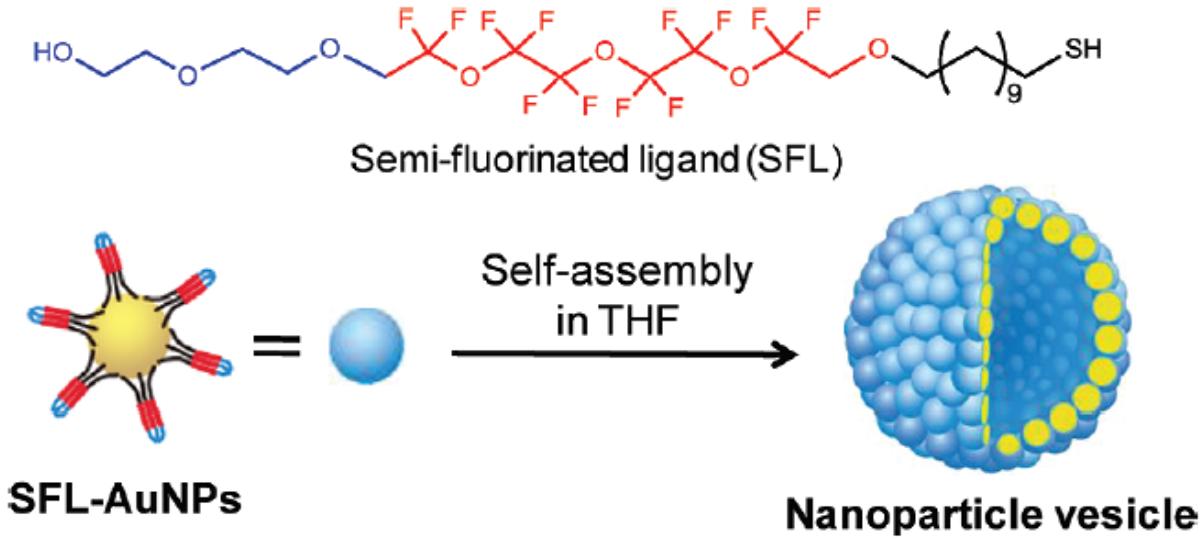

5, 10, 20 nm

the solvophobic feature of the fluorinated bundles is the driving force for NP assembly

K. Niikura *et al. J. Am. Chem. Soc.* **2012**, *134*, 7632.

synthesis of water-soluble fluorinated Au NPs

Synthesis

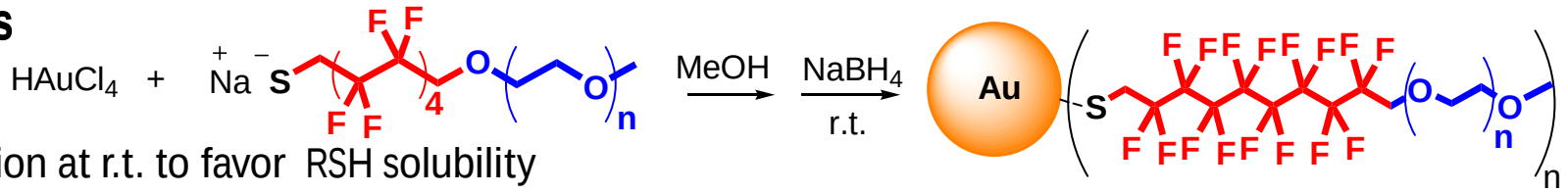

- ✧ reaction at r.t. to favor RSH solubility
- ■ for n= 3, 4 and 6 NPs precipitate in MeOH, they are scarcely soluble in DCM and chloroform

RSH/Au	NP core average diameter (nm)	
0.7	2.9	
2	2.7	average composition: $Au_{670}(SF8PEG)_{107}$
2.5	1.6	

- ■ NPs are soluble in water, methanol, DCM and chloroform

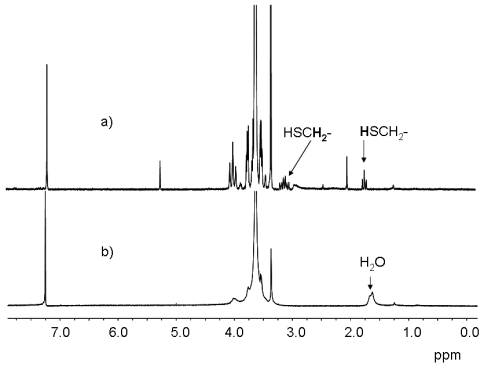

(a) ^{1}H NMR of HS-F8-PEG and (b) ^{1}H NMR of MPC-F8-PEG prepared with a thiol/Au ratio of 2:1.

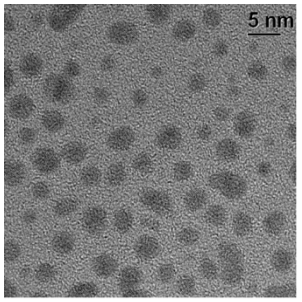

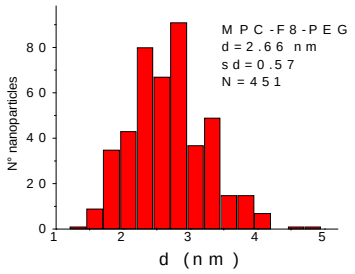

TEM image and histogram of MPC-F8-PEG.

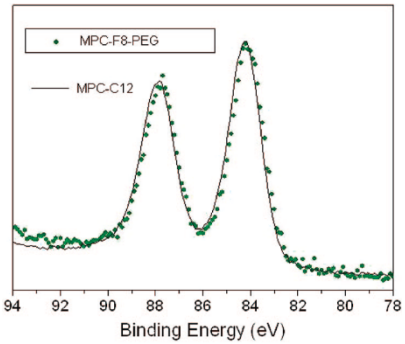

XPS Au 4f core level spectra of MPC-F8-PEG and MPC-C12.

C. Gentilini, F. Evangelista, P. Rudolf, P. Franchi, M. Lucarini, L. Pasquato *J. Am. Chem. Soc.* **2008**, *130*, 15678-15682.

synthesis of Au NPs capped by a mixture of H- and F- thiolates

- *Homogeneous phase synthesis (methanol/water) using mixtures of thiolates with **immiscible chains***

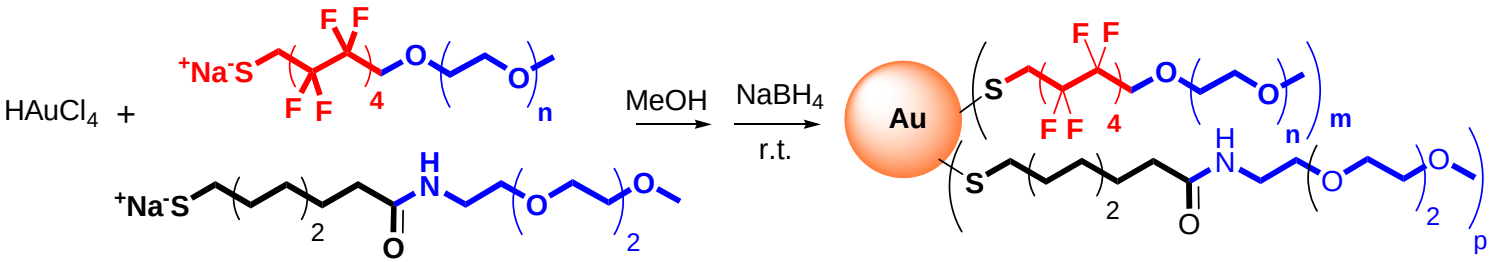

n = 10,11

NP-C8-TEG/F8-PEG

- *synthesis of mixed-monolayer by exchange reaction*

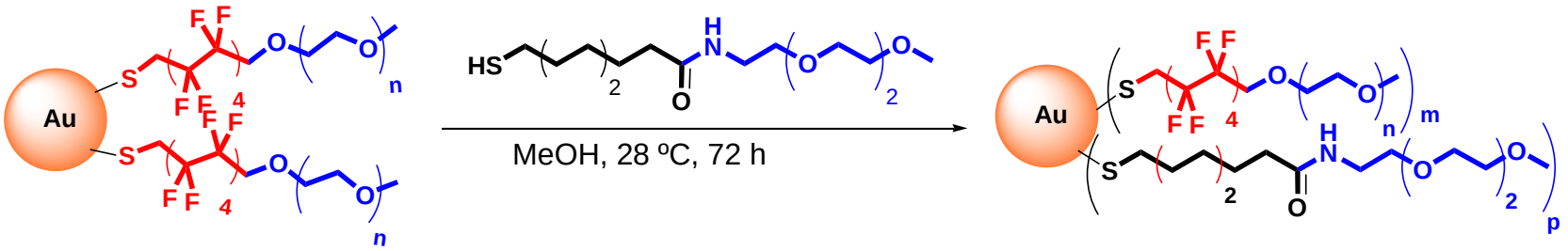

NP-F8-PEG

NP-C8-TEG/F8-PEG

C. Gentilini, P. Franchi, E. Mileo, S. Polizzi, M. Lucarini, L. Pasquato Angew. Chem. Int. Ed. ***2009****, 48, 3060.*

gold nanoparticles protected by amphiphilic fluorinated ligands

ESR studies

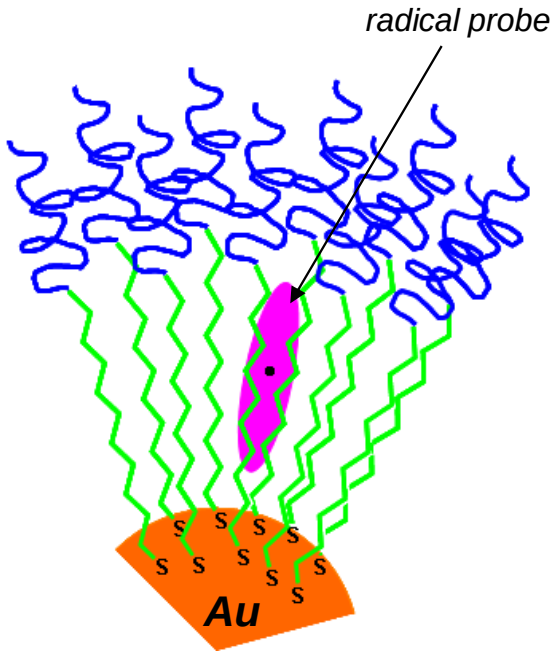

perfluorinated alkyl chain

poly(oxoethylene) chain

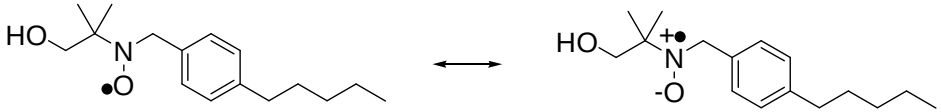

radical probe

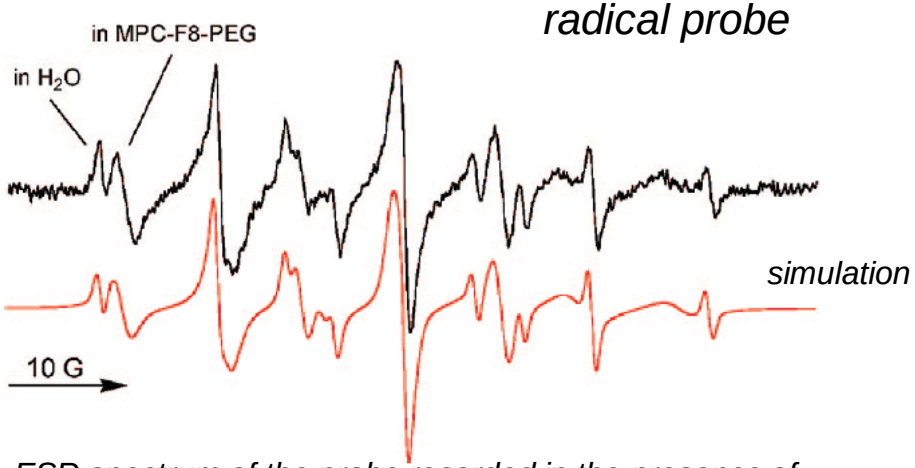

ESR spectrum of the probe recorded in the presence of NP-F8-PEG 0.56 mM (in black) and the corresponding computer simulation (in red).

ESR parameters of the radical probe (1 G = 0.1 mT) and partition equilibrium (K_{eq}) constants at 298 K.

	***a*(N)/G**	***a*($2H_\beta$)/G**	***g*-factor**	K_{eq} / M^{-1}
water[a]	16.25	10.14	2.0056	—
NP-F8-PEG	15.46	8.68	2.0057	176
NP-C8-TEG	15.67	8.97	2.0057	87[c]

[a] Contains 10% (v/v) of methanol.

C. Gentilini, F. Evangelista, P. Rudolf, P. Franchi, M. Lucarini, L. Pasquato J. Am. Chem. Soc. ***2008****, 130, 15678-15682.*

gold nanoparticles protected by H-/F- mixed-monolayers

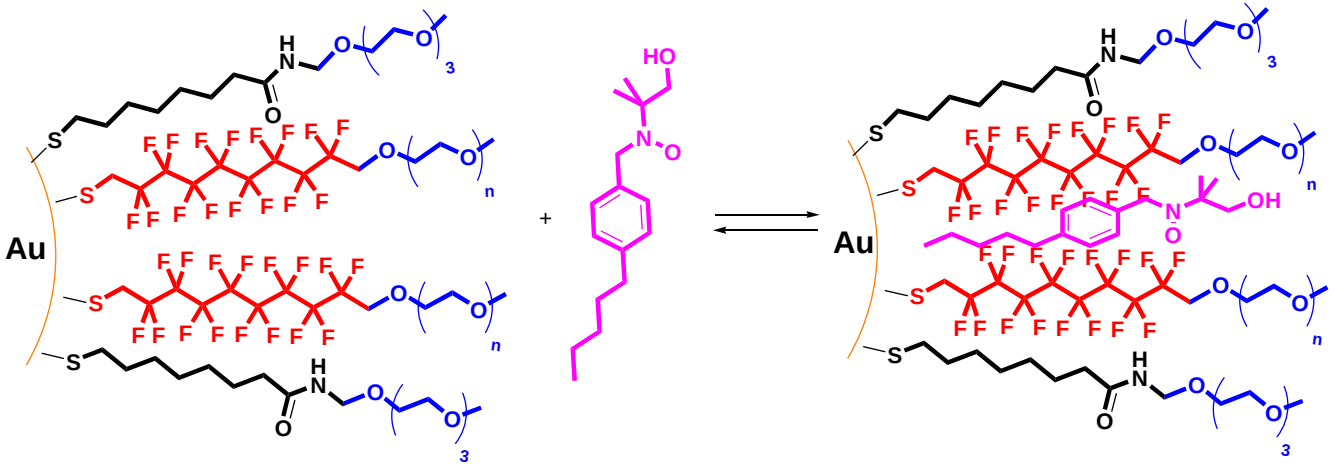

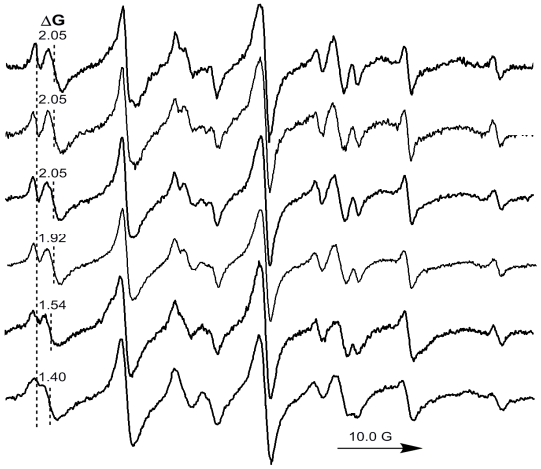

NP-F8-PEG

R_{SAM} *1*

R_{SAM} *2.5*

R_{SAM} *4*

R_{SAM} *20*

NP-C8-TEG

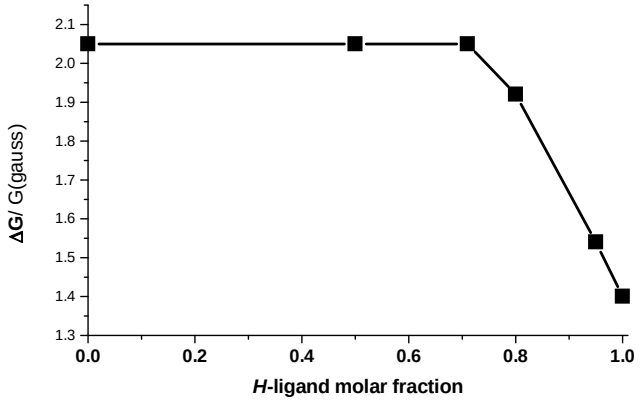

C. Gentilini, P. Franchi, E. Mileo, S. Polizzi, M. Lucarini, L. Pasquato Angew. Chem. Int. Ed. ***2009****, 48, 3060.*

gold nanoparticles protected by H-/F- mixed-monolayers

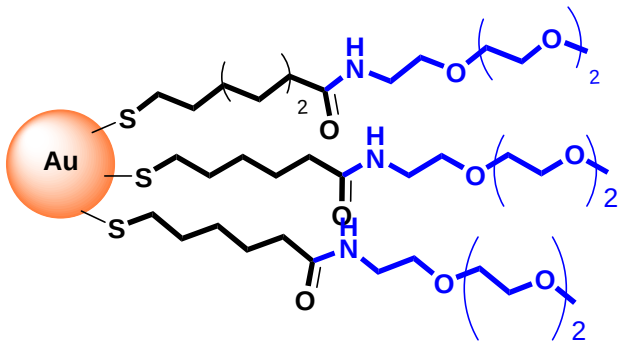

NP-C8-TEG

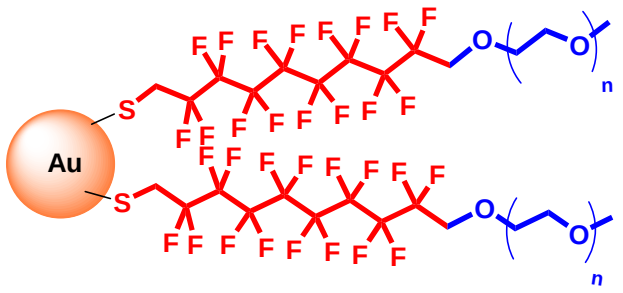

NP-F8-PEG

ESR Parameters in the Presence of Homoligand NP Mixtures

χ	$[3]_{monolayer}/[3]_{water}$ [b]	$\Delta G/G$ [c]
0	9.9 (9.8)	2.05 (2.05)
0.5	8.1 (7.8)	1.90 (1.82)
0.71	7.4 (7.1)	1.84 (1.69)
0.80	6.7 (6.5)	1.68 (1.60)
0.95	6.0 (6.1)	1.50 (1.45)
1	6.0 (6.0)	1.45 (1.40)

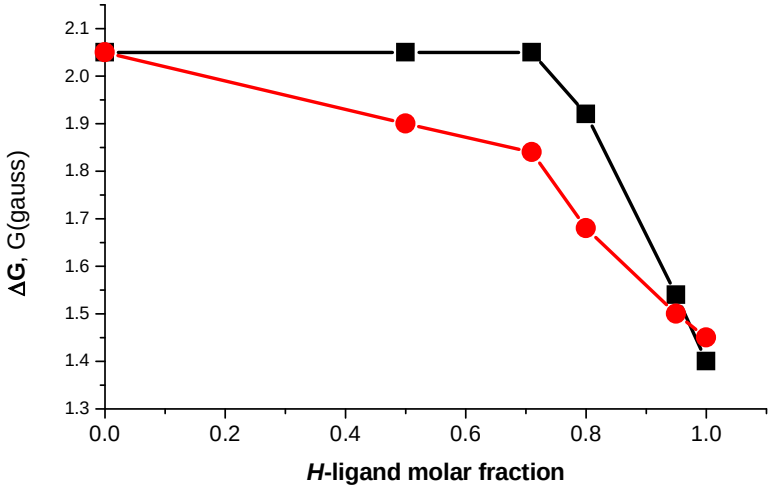

P. Posocco, et al., ACS Nano ***2012****, 6, 7243-7253.*

gold nanoparticles protected by H-/F- mixed-monolayers

Mesoscopic simulations details

in collaboration with Sabrina Pricl Paola Posocco and Maurizio Fermeglia

- ✓ *Self-assembled organization was predicted at the nanoscale using corse grained (CG) simulations in presence of solvent*
- ✓ *CG calculations allow to reach time and length scales larger than classical atomistic predictions and closer to those involved in the experimental phenomena*
- ✓ *An ad hoc multiscale molecular modeling procedure was developed. It employs the information obtained from atomistic molecular dynamics simulation to parametrize mesoscale dissipative particle dynamics (DPD) models, thus incorporating all chemical details even at the CG level*

*L. Pasquato et al., ACS Nano **2012**, 6, 7243-7253.*

gold nanoparticles protected by H-/F- mixed-monolayers

multiscale molecular simulation: validation of the procedure

Au NP with a core size of 4.5 nm coated by a mixture of 2:1 of MUS and OT ligands (F. Stellacci et al. Chem. Commun. 2008, 196.)

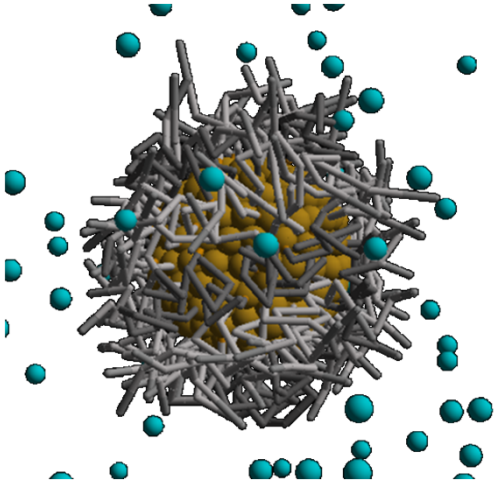

MUS

OT

water

gold core

Rippled morphology predicted using a multiscale approach.

*L. Pasquato, et. al. ACS Nano **2012**, 6, 7243-7253.*

gold nanoparticles protected by H-/F- mixed-monolayers

multiscale molecular simulation

Ligand organization on the surface of gold NPs at different molar fraction of the two ligands

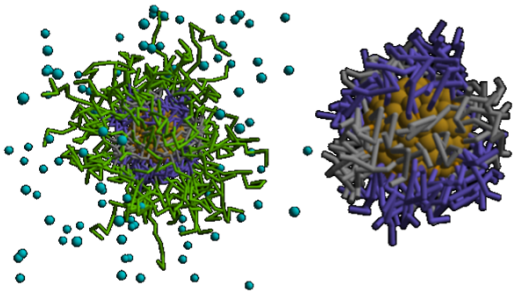

χ_H = 0.50, ∅ 2.2 nm

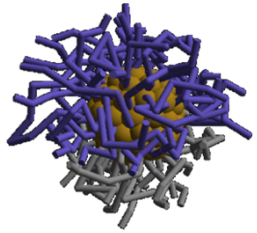

χ_H = 0.50, ∅ 1.6 nm

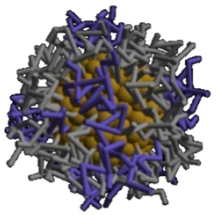

χ_H = 0.71, ∅ 2.5 nm

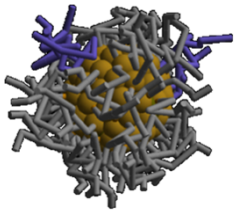

χ_H = 0.80, ∅ 1.9 nm

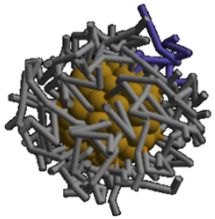

χ_H = 0.95, ∅ 1.9 nm

*L. Pasquato, et al. ACS Nano **2012**, 6, 7243-7253.*

drug loading by mixed-SAMs

Equilibrium constants in the presence of heteroligand mixed-monolayers as determined from ESR measurements

***H*-ligand molar fraction**	K_F^a/M^{-1}
0	176
0.50	200
0.71	350
0.80	762
0.95	600
1.0	-

atomistic and mesoscale calculations

		Shell thickness (nm)
Homoligand NPs	F8PEG	2.82
	C8TEG	1.40
Heteroligand NPs	F8PEG	2.60
	C8TEG	1.59

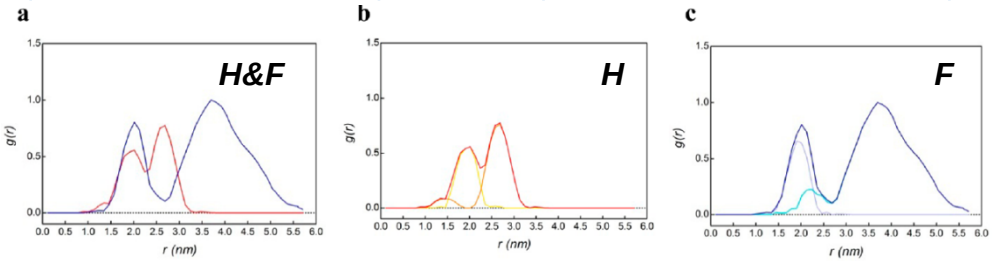

Radial distribution functions (RDFs) for the SAM components of MPC-C8-TEG/F8-PEG, 1:1.

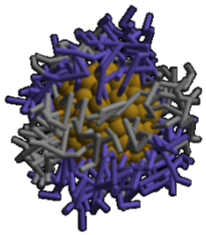

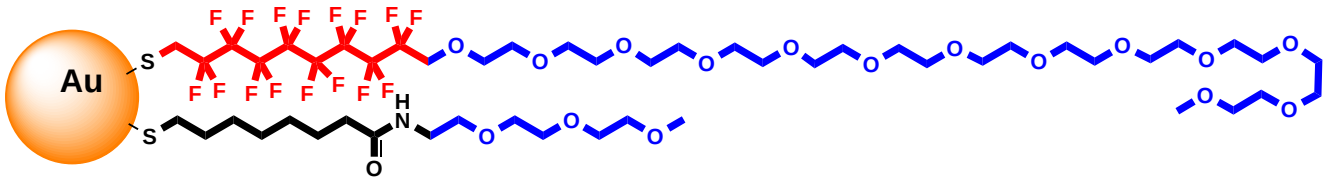

*L. Pasquato et al., ACS Nano **2012**, 6, 7243-7253.*

Surface properties of proteins

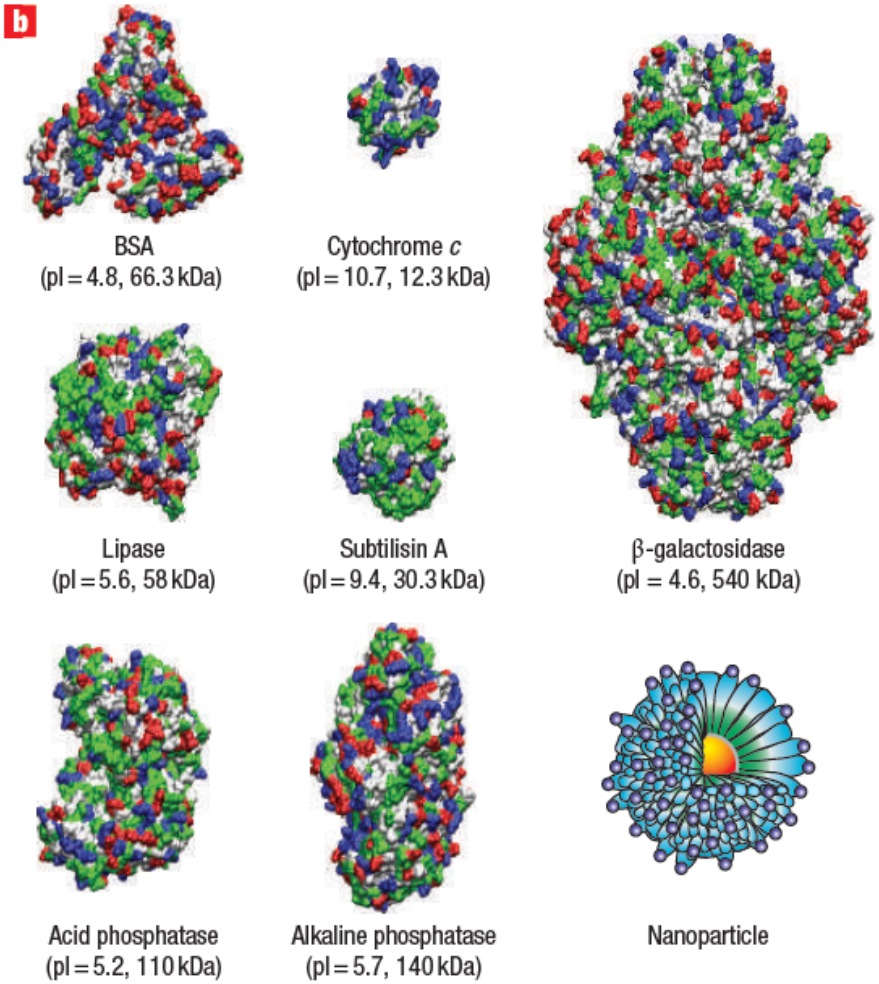

Colour scheme for the proteins: nonpolar residues (grey), basic residues (blue), acidic residues (red) and polar residues (green).

C.-C. You et al. Nature Nanotech. 2007

the mechanism of membrane penetration and toxicity depends on surface structure

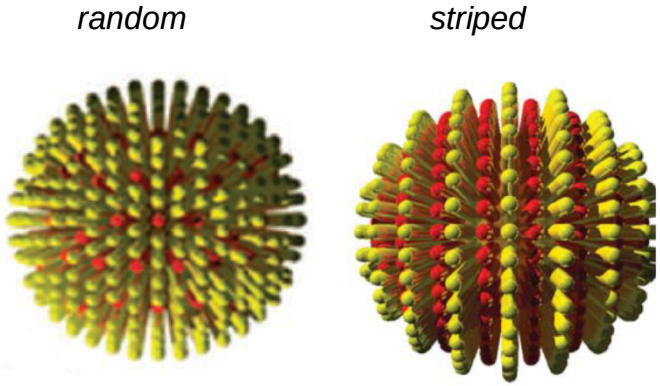

A. Verma et al. Nature Mater. 200
S. Sabella et al. Nanoscale 2014

Effect of the NP surface morphology on cellular uptake and toxicity

Surface-structure-regulated cell-membrane penetration by monolayer-protected nanoparticles

AYUSH VERMA[1], OKTAY UZUN[1], YUHUA HU[2], YING HU[1], HEE-SUN HAN[3], NICKI WATSON[4], SUELIN CHEN[1], DARRELL J. IRVINE[1,5]* AND FRANCESCO STELLACCI[1]*

Nature Mater. 2008

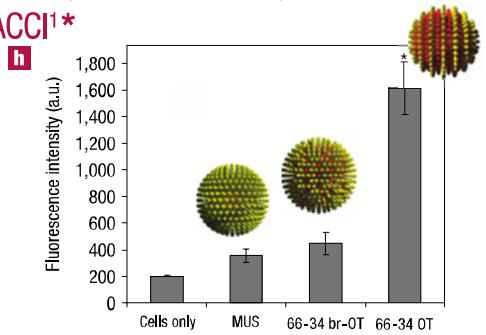

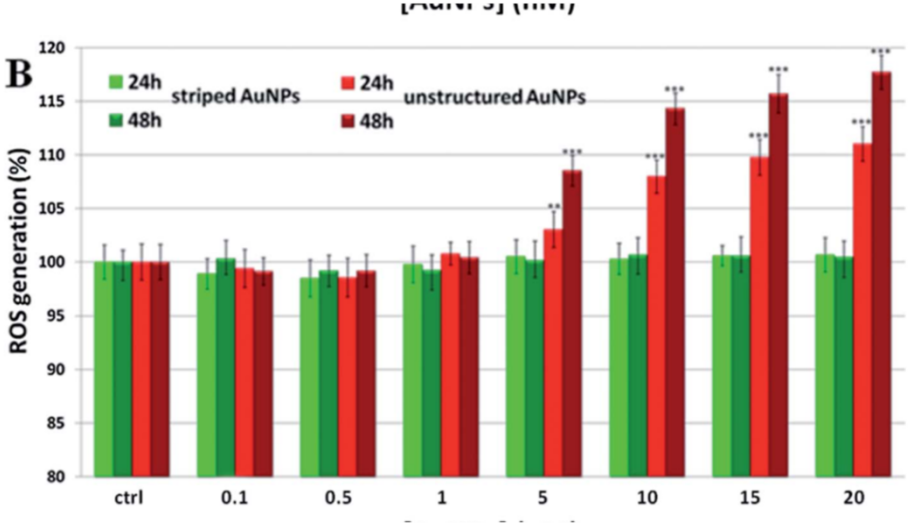

S. Sabella et al. Nanoscale, 2014, 6, 7052

Interaction of Nanoparticles with cells

system 1

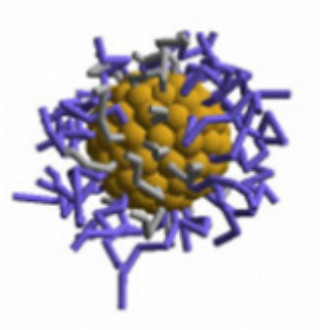

striped-NPs
core diam. 1.9 nm
NP diam. ~ 7.1 nm
$Au_{260}(C8TEG)_{20}(F8PEG)_{36}$

system 2

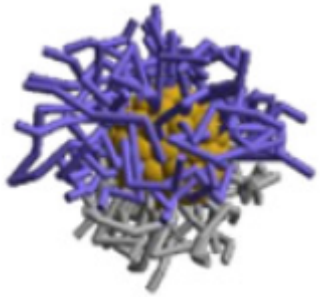

Janus-NPs
core diam. 1.6 nm
NP diam. ~ 6.8 nm
$Au_{140}(C8TEG)_{24}(F8PEG)_{32}$

credits to: Alessandro Tossi
Sabrina Pacor
Milena Guida

- three types of cells:

U937 – leukemia cells
MEC-1 – lymphoma cells
A549 – lung adenocarcinoma

- tests for mitocondrial activity: DiOC6/PI and JC-1
- MTT: cell proliferation test to evaluate toxicity

- Biacore experiments to have evidence of the interaction with liposomial membrane

Citotoxicity: MTT test

MEC-1 cells, complete medium, 24h

credits to: Alessandro Tossi
Sabrina Pacor
Milena Guida

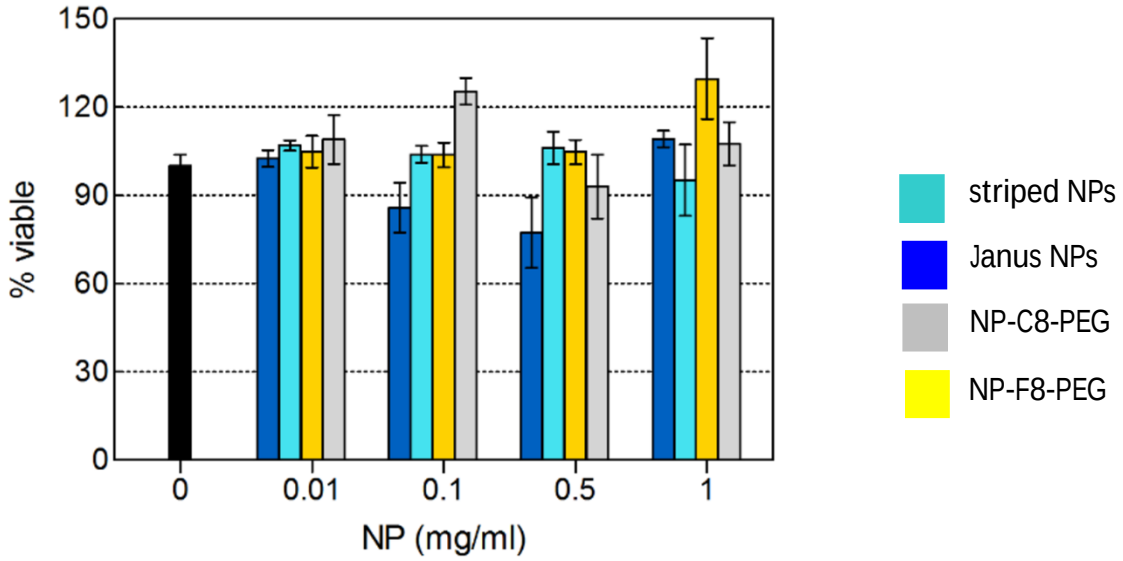

Cytotoxicity of NPs treated cells. MEC-1 cells viability, evaluated by MTT assay, after 24h treatm concentrations indicated on x-axes; data are expressed as mean ± SEM of the measured O.D. of at least three times and performed at least in triplicate.

L. Pasquato, P. Posocco, *Small 2019*.

Mitochondrial activity

evaluation of apoptotic damage to mitochondrial functionality

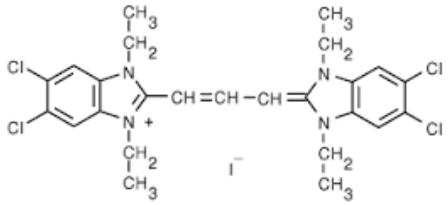

JC-1 mitochondrial potential sensor

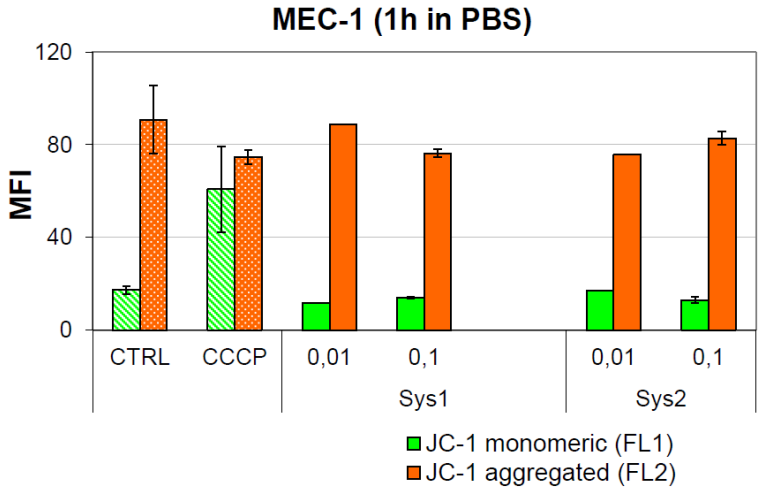

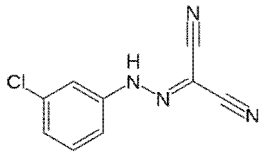

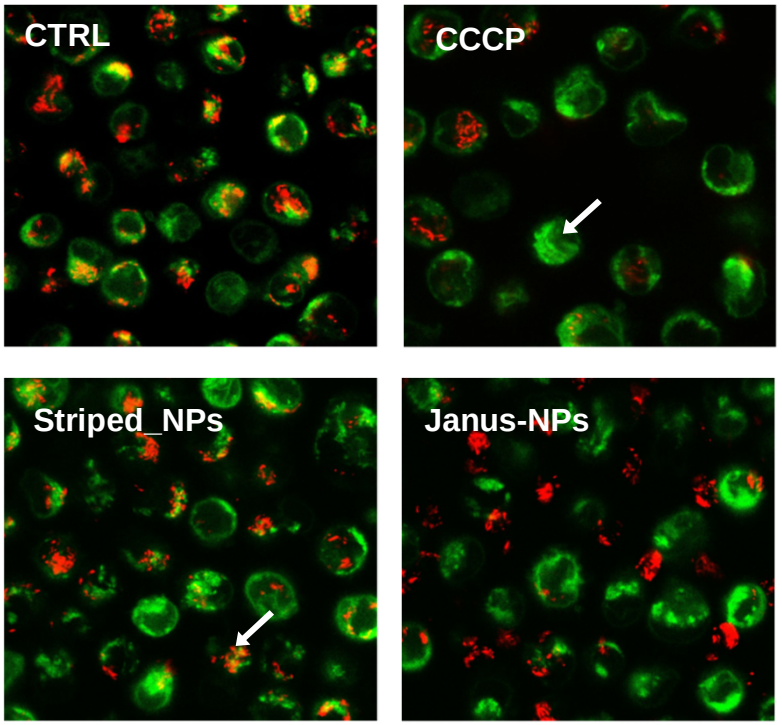

Flow cytometry: Striped- and Janus- GNP did not cause the orange fluorescence of treated cells with respect to untreated controls.

Confocal microscopy: only the positive control caused disaggregation, conc. 0.1 mg/ml.

GNPs do not cause mitochondrial damage

L. Pasquato, P. Posocco, *Small 2019*.

cell internalization of NPs

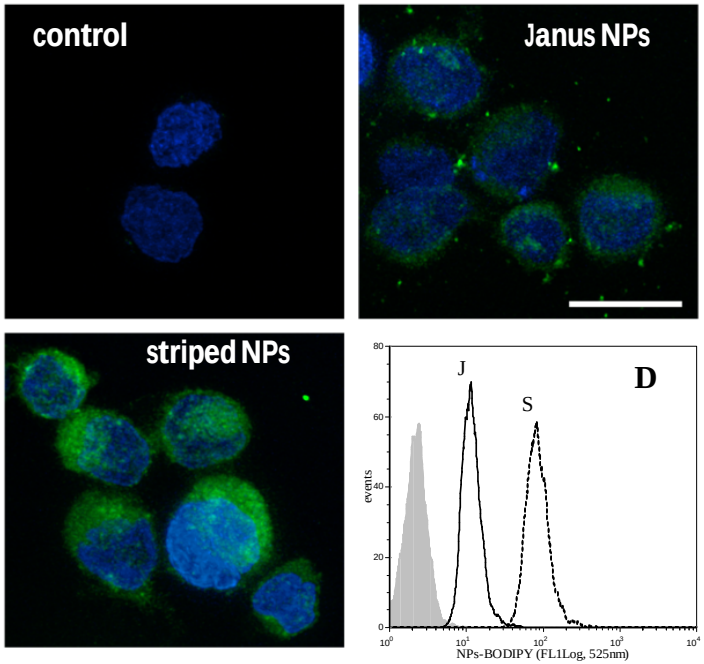

Janus and striped NPs cross the plasma membrane and reach the cytoplasm

internalization is favoured by the stripe-like morphology of the monolayer.

MEC-1 cells treated with **BODIPY-tagged NPs**. **A**) Confocal images of control cells, **B**) cells trea Janus NP and **C**) cells treated with 0,1 mg/ml striped, for 60 min prior to counterstaining nuc Panel **D** represents the flow cytometric overlay of green fluorescence emitted from untreate BODIPY-NP treated cells, 1mg/ml Janus (J) and 0,1 mg/ml striped (S).

L. Pasquato, P. Posocco, *Small 2019*.

SPR Experiments – binding NPs-model membranes

The sensor surface is dextran coated, chip L1
Liposomes of DOPC

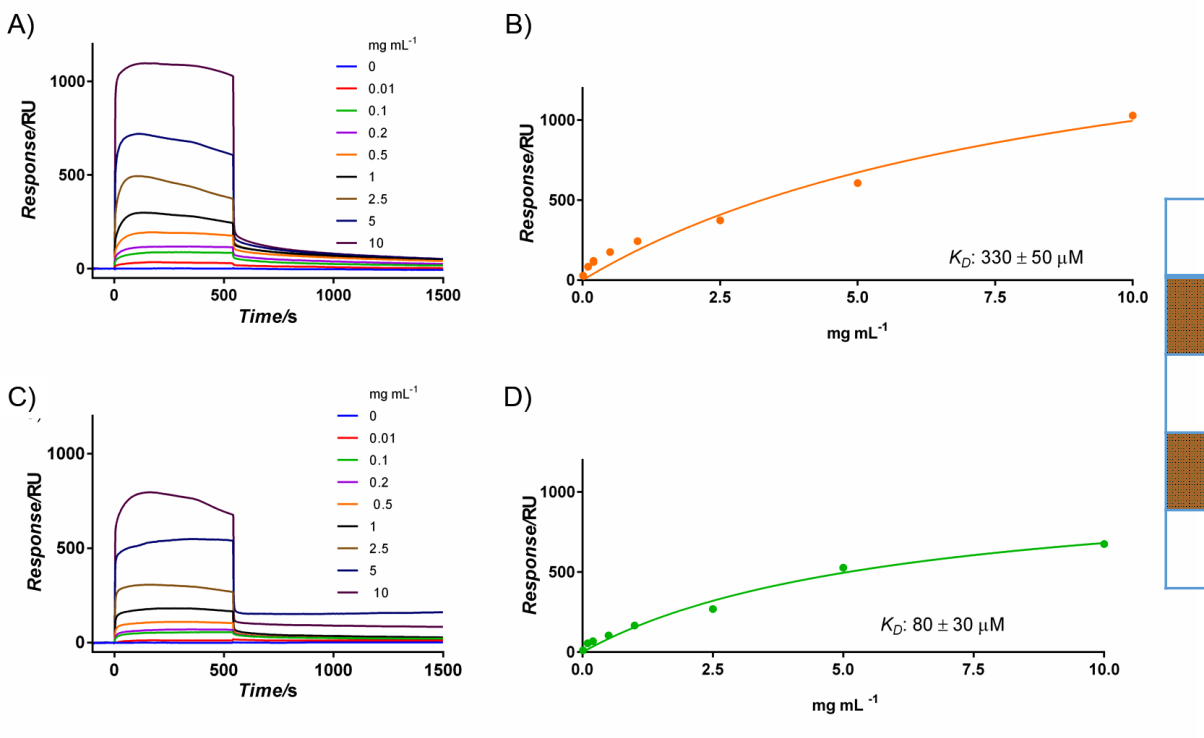

Nanoparticles	K_{diss}, µM
NP-striped	80 ± 28
NP-Janus	330 ± 50
NP-F8-PEG	60 ± 50
NP-C8-PEG	118 ± 50

L. Pasquato, P. Posocco, *Small 2019*.

Computational studies of NP-membrane interaction by MARTINI mapping

Paola Posocco
Domenico Marson

Nanoparticle/ composition	ΔG_{adh} [kcal/mol]	$N_{contacts}$	% contacts non-PEG component	% contacts PEG component
NP-Striped	-38.9 ± 1.0	25 ± 1	37	63
NP-Janus	-28.6 ± 1.5	21 ± 2	41	59
NP-F8-PEG	-51.0± 1.2	32 ± 2	27	73
NP-C8-PEG	-44.1 ± 0.8	31 ± 2	28	72

Detachment of NP from the membrane by «umbrella sampling»

L. Pasquato, P. Posocco, *Small 2019*.

Role of fluorintated ligands in the interaction with biological structures

Perfluoroalkylchain conjugation as a new tactic for enhancing cell permeability of peptide nucleic acids (PNAs) via reducing the nanoparticle size

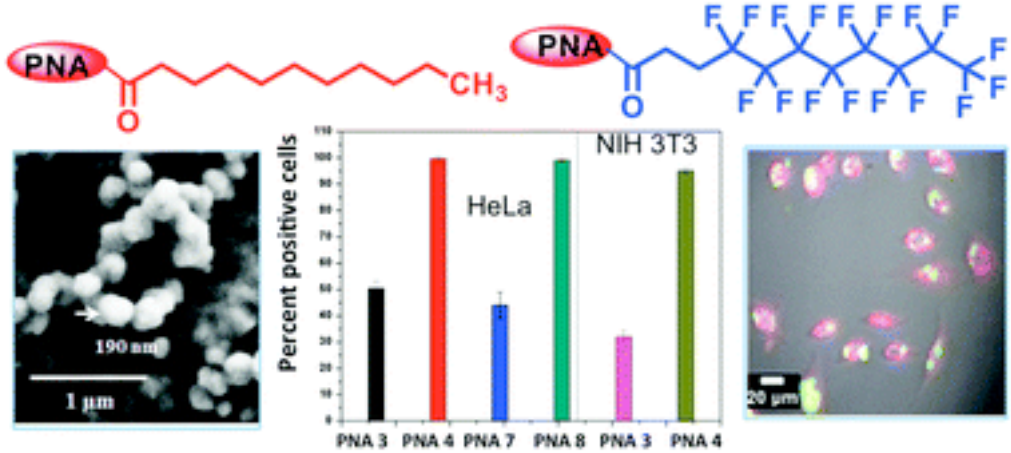

S. Ellipilli et al. Chem. Commun. 2016

drug loading - influence of the monolayer properties

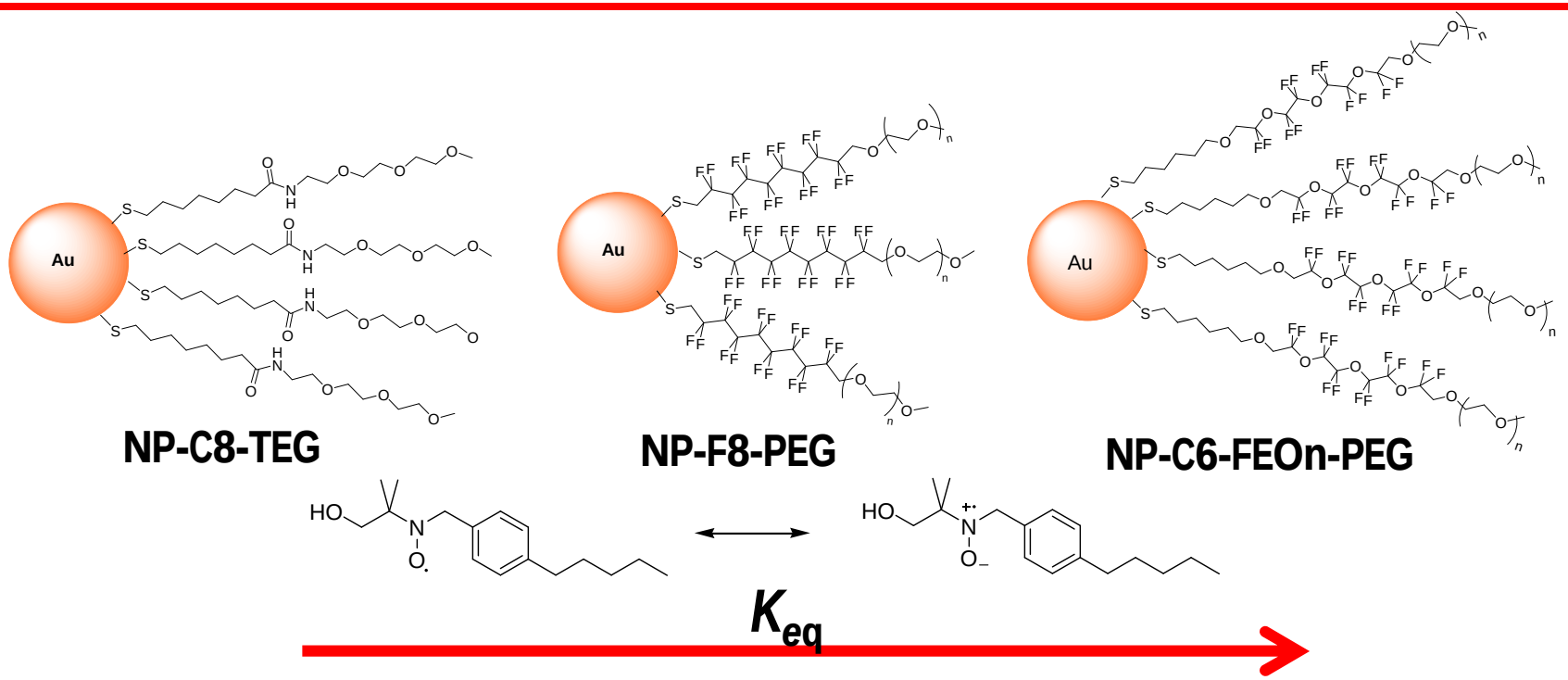

	a(N)/G	$a(2H_\beta)$/G	g-factor	d core	K_{eq}/M^{-1}
Water	16.25	10.14	2.0056	-	-
NP-C8-TEG	15.67	8.97	2.0057	1.6 nm	104
NP-F8-PEG	15.46	8.68	2.0057	2.7 nm	176
NP-C6-FEOn-PEG	**15.45**	**8.65**	**2.0057**	**1.4 nm**	**593**

L. Pasquato et al. J. Mater. Chem. 2015, 3, 432-439.

drug loading - *H*- vs. *F*-monolayer

- desolvation energy
- hydrophobic interactions
- halogen bonds

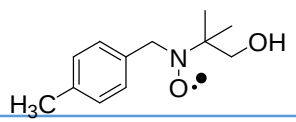

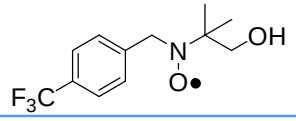

	K_{eq} / M^{-1}		K_{eq} / M^{-1}		$K_{eq}(F)/K_{eq}(H)$
NP-C8-TEG	2.2	2.6	4	7.2	1.8
NP-F8-PEG	5.7		29		5.1
NP-FEO$_n$-PEG	16	2.8	100	3.4	6.2

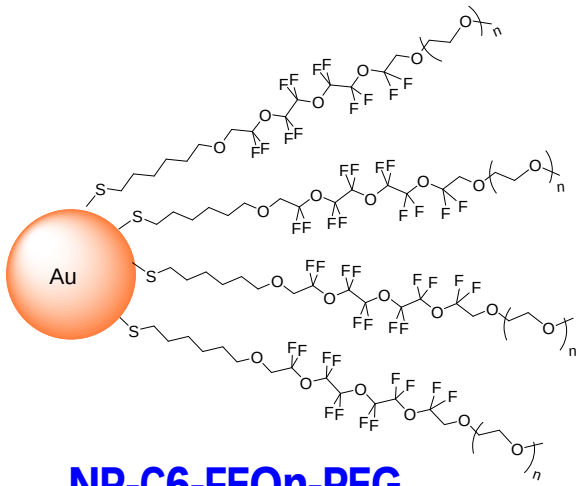

NP-C6-FEOn-PEG

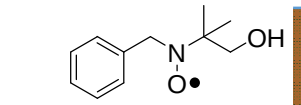

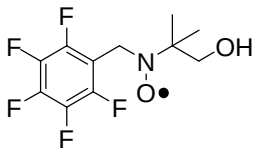

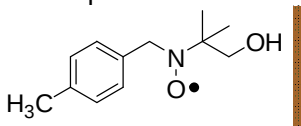

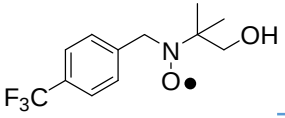

K_{eq} / M^{-1}	$K_{eq}(F)/K_{eq}(H)$
6.2	12.9
80	
16	6.25
100	

L. Pasquato et al. J. Mater. Chem. 2015, 3, 432-439.

release of the drug

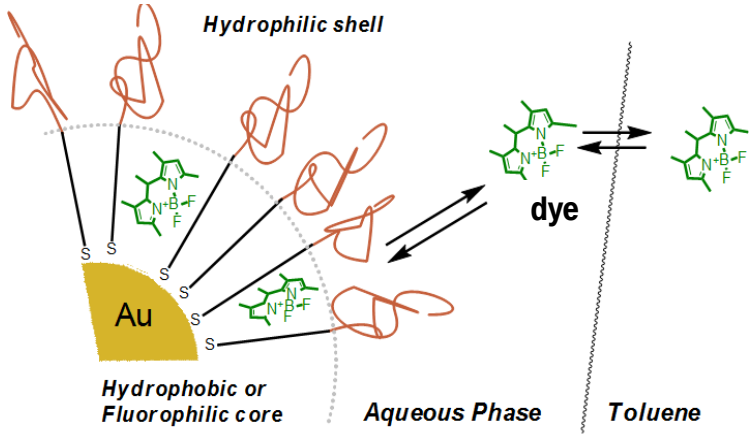

NP	k_1, s^{-1}	k_2, s^{-1}	[NPs], µM	[dye], µM
None	0.03	-	-	0.168
NP C8PEG	0.02	2×10^{-4}	0.426	0.168
NP F8PEG	5×10^{-3}	-	0.632	0.168
NP C6OFPEG 3 nm	0.02	5×10^{-4}	0.229	0.153
NP C6OFPEG 1.4 nm	0.03	4×10^{-4}	1.15	0.168

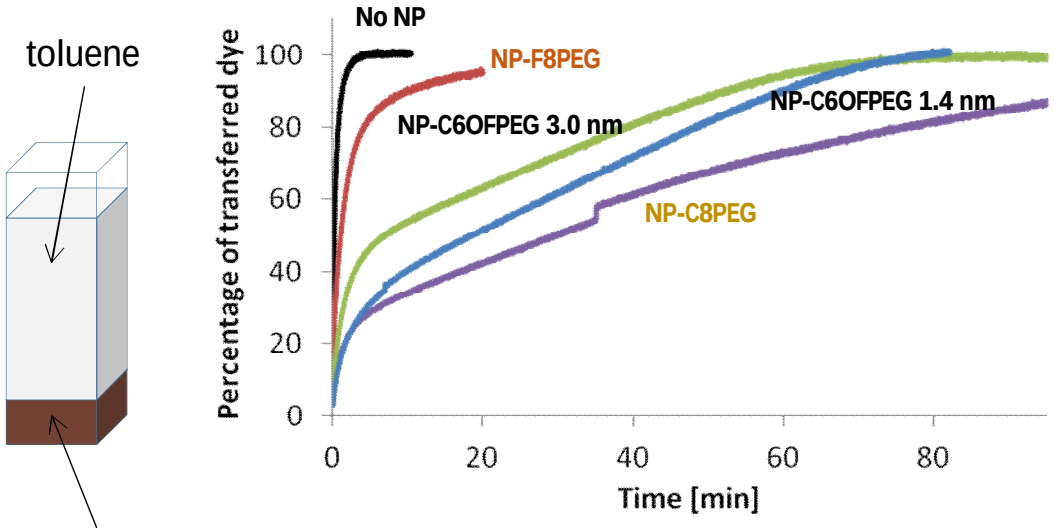

Bodipy solution (µM) in the presence of NPs (µM)

Effect of the NPs monolayers on the phase transfer rate of the hydrophobic fluorescent bodipy dye from an aqueous solution containing NPs to a toluene layer.

L. Pasquato et al. J. Mater. Chem. 2015, 3, 432-439.

GNPs for ^{19}F MRI

design, synthesis and use of gold NPs protectected by fluorinated ligands as nanomaterial for imaging and therapy

modular system

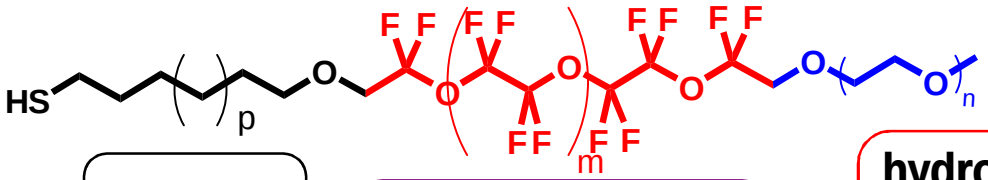

spacer stability

^{19}F active chain for MRI

hydrophilic chain to impart solubility in biological media

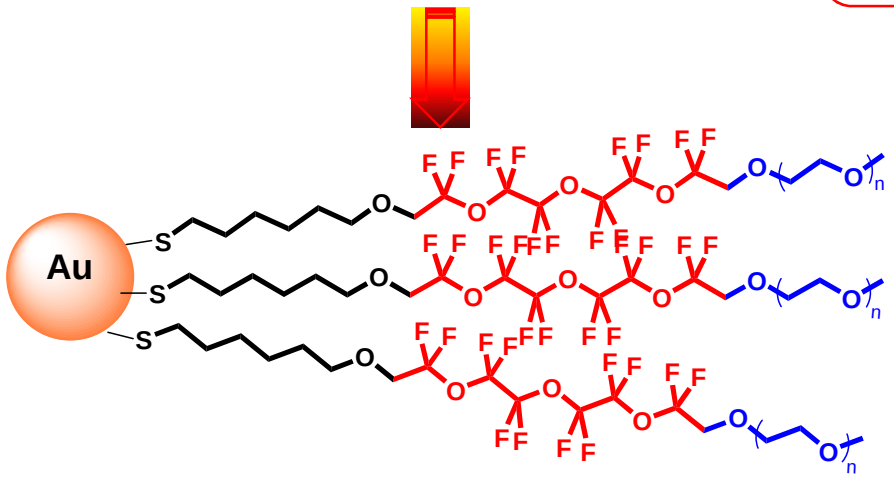

n = 3

n = 12-13 (PEG550)

L. Pasquato et al. *Chem. Commun.* **2013**, *49*, 8794.

GNPs for ^{19}F MRI

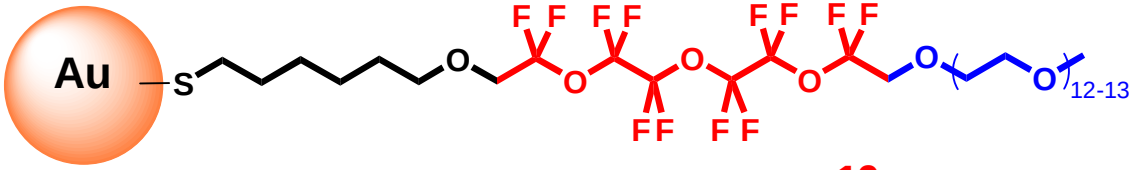

^{1}H NMR

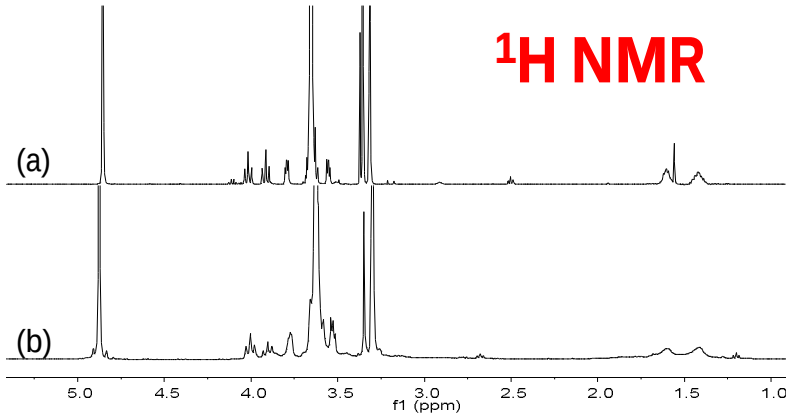

^{1}H NMR (500 MHz, CD_3OD) of thiol (a) and MPC C6-OF-PEG (b).

^{19}F NMR

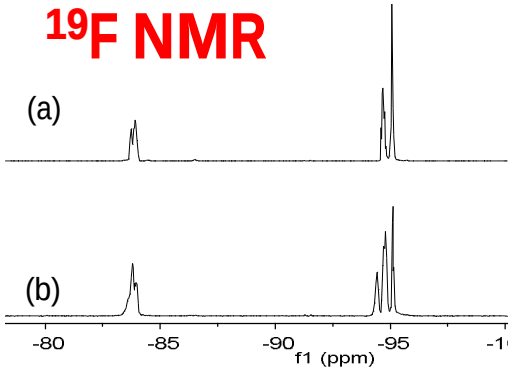

^{19}F NMR (500 MHz, CD_3OD) of protected thiol (a) and MPC C6-OF-PEG (b).

UV-Vis

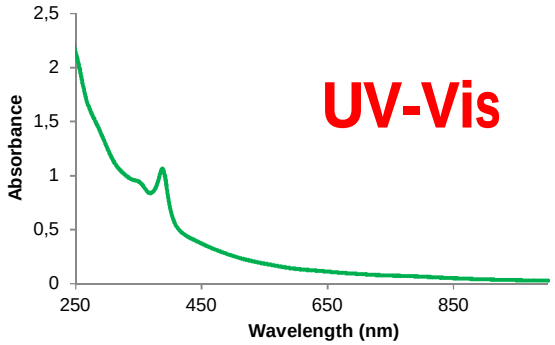

UV-Vis spectrum in methanol.

TGA

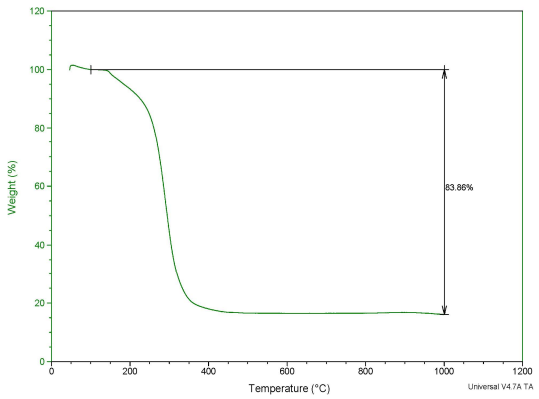

GNPs for ^{19}F MRI

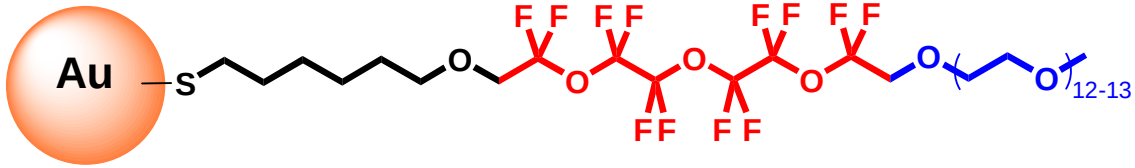

TEM

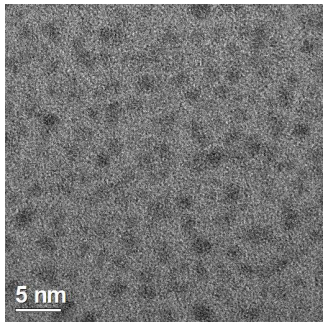

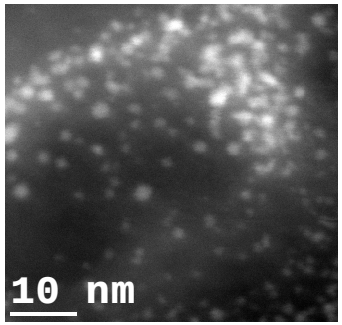

STEM-HAADF

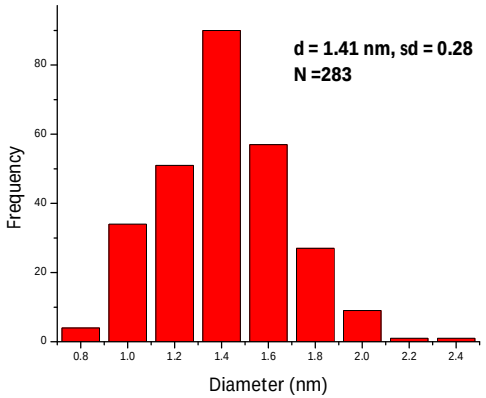

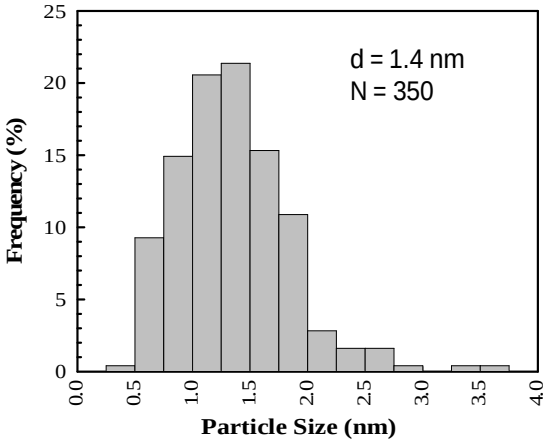

Juan J. Delgado, Univ. de Cádiz, Spain

GNPs for ^{19}F MRI

NMR/MRI

Relaxation times (^{19}F-NMR)

T1 (spin-lattice relaxation time)
Inversion Recovery

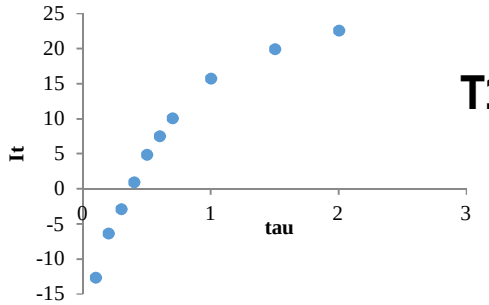

T1 = 588 ms

T2 (spin-spin relaxation time)
CPMG sequence
(Carr-Purcell Meiboom-Gill)

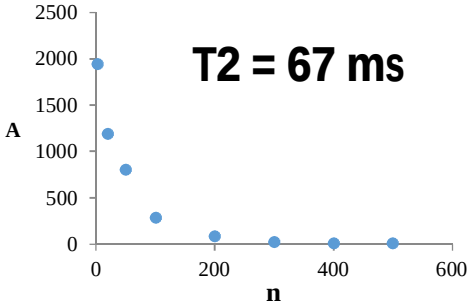

T2 = 67 ms

^{19}F-MR images

18.75 mg/mL of NPs (6.06x10^{19} ^{19}F/mL)

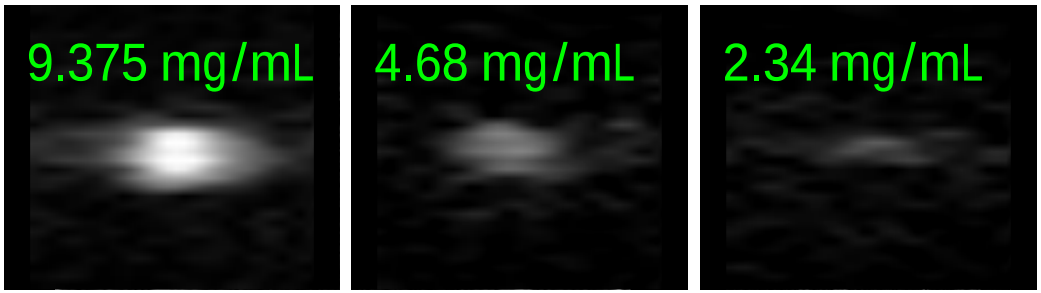

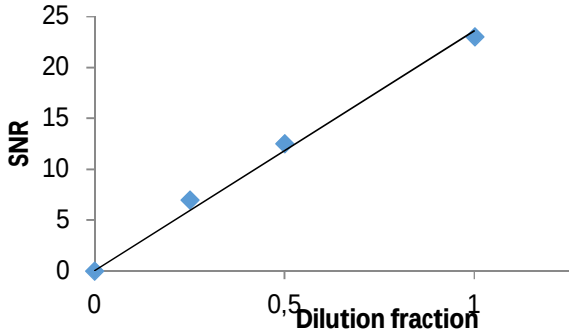

L. Pasquato et al. *Chem. Commun.* **2013**, *49*, 8794.

NP-C6-FEO-PEG, cellular uptake

4 h incubation with HeLa cells at 37 ºC, and 30 min RBC

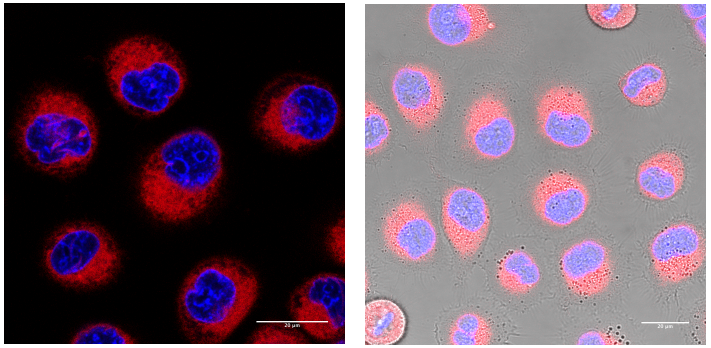

Confocal laser microscopy images of HeLa cells (nucleus stained in blue, Hoechst dye) loaded with F-MPCs **4b** (red fluorescent signal) for 4 h at 37 °C.

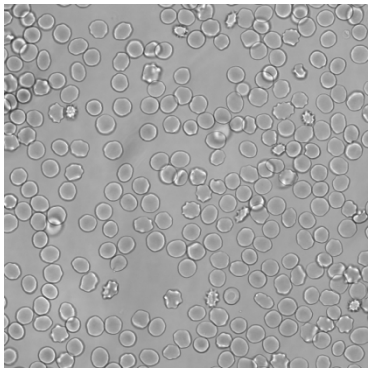

RBCs do not uptake NPs only free dye is able to penetrate their cell membrane or remain attached to the membrane.

No unbound Bodipy was detected by RBC test.

4 h incubation with HeLa cells at 4 ºC (endocytic/ pinocytic mechanisms are arrested)

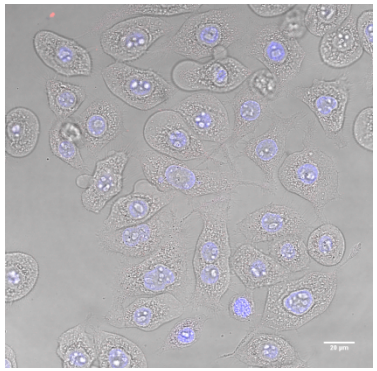

No visible red signal, only very little is possible visualized with the enhanced signal.

F. Sousa, IEO, Milan

NP-C6-FEO-PEG, cellular viability

UL – dead cells not labeled with NPs
UR - dead cells labeled with NPs
LL – viable cells not labeled with NPs
LR- viable cells labeled with NPs

FACS for PI of HeLa incubated 4 hrs with MPC C6-FEO-PEG

PI

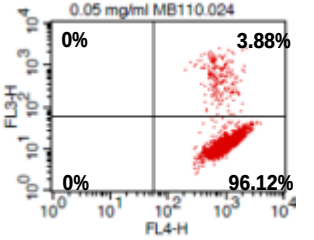

Quad	% Gated	% Total	X Mean	Y Mean
UL	0.00	0.00	***	***
UR	3.88	3.76	837.01	664.12
LL	0.00	0.00	***	***
LR	96.12	93.20	1039.46	13.15

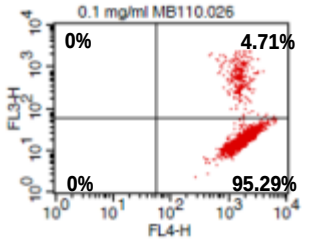

Quad	% Gated	% Total	X Mean	Y Mean
UL	0.00	0.00	***	***
UR	4.71	4.58	1637.27	750.07
LL	0.00	0.00	***	***
LR	95.29	92.67	1811.77	17.82

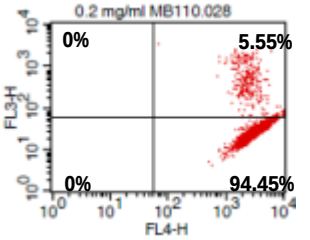

Quad	% Gated	% Total	X Mean	Y Mean
UL	0.00	0.00	***	***
UR	5.55	5.41	3212.32	615.86
LL	0.00	0.00	***	***
LR	94.45	91.97	3016.69	24.87

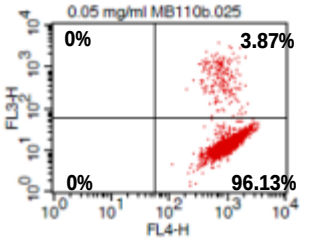

Quad	% Gated	% Total	X Mean	Y Mean
UL	0.00	0.00	***	***
UR	3.87	3.76	856.39	714.69
LL	0.00	0.00	***	***
LR	96.13	93.37	1053.28	13.30

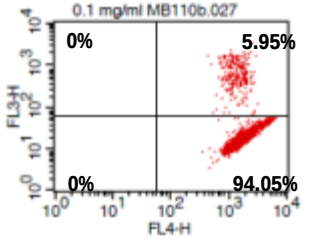

Quad	% Gated	% Total	X Mean	Y Mean
UL	0.00	0.00	***	***
UR	5.95	5.78	1466.03	756.91
LL	0.00	0.00	***	***
LR	94.05	91.43	1859.41	18.15

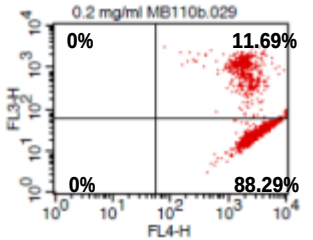

Quad	% Gated	% Total	X Mean	Y Mean
UL	0.00	0.00	***	***
UR	11.69	11.19	2331.72	932.99
LL	0.02	0.02	1.63	2.59
LR	88.29	84.56	3067.29	25.01

The percentage of viable cells is above **95%** after taken up NPs. The percentage of dead cells labeled with NPs are very similar to all concentrations tested.

second generation GNPs for ^{19}F MRI

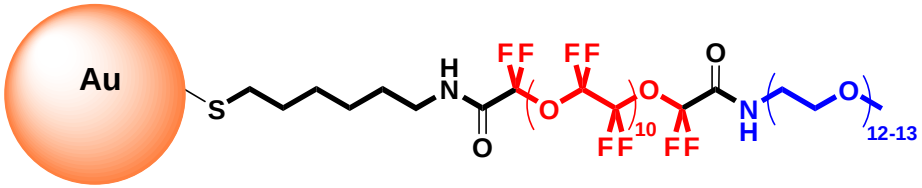

excellent solubility in water

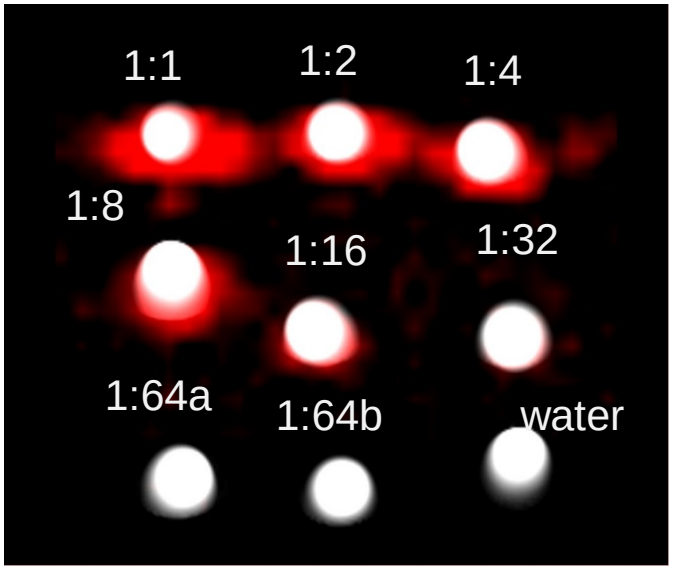

^{1}H (white) and ^{19}F MRI (red).

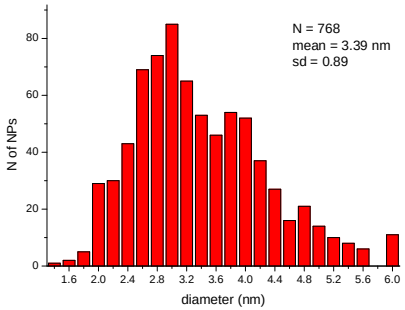

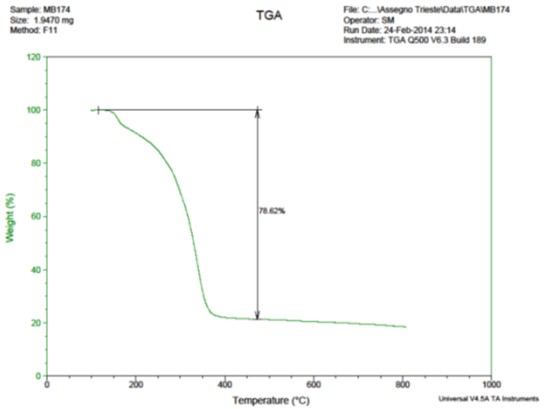

in solution of 1 mg/ml T1 = 490 ms

T2 = 15.34 ms

T2* = 0.41

second generation GNPs for ^{19}F MRI

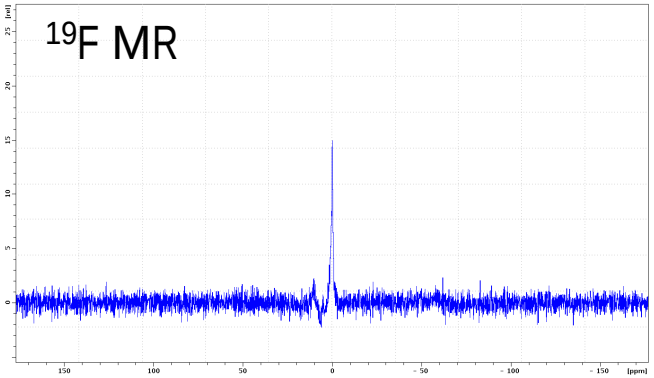

7 Tesla

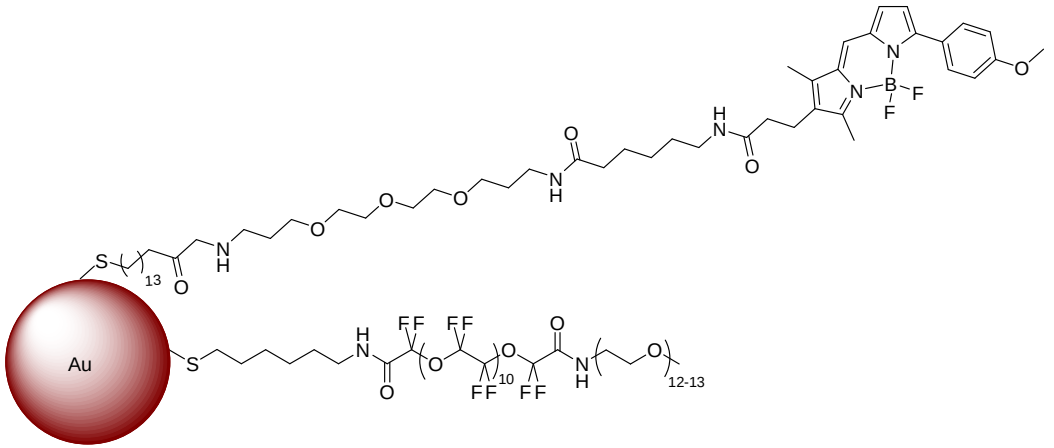

^{19}F MRI

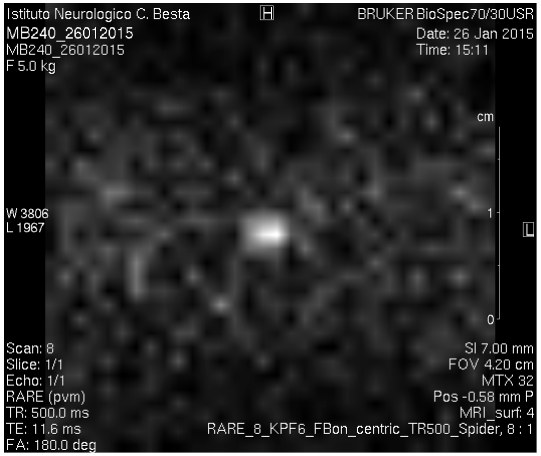

T1 = 455.67 ± 11.44 ms

T2 = 29.75 ± 2.52 ms

T2* = 1.45 ± 0.22 ms

1 μL of solution 8.4 mg/mL, 1 h acquisition time

ANISOTROPIC METAL NANOPARTICLES

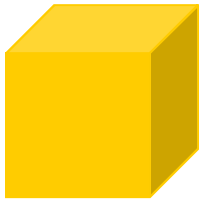

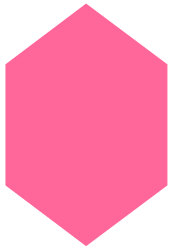

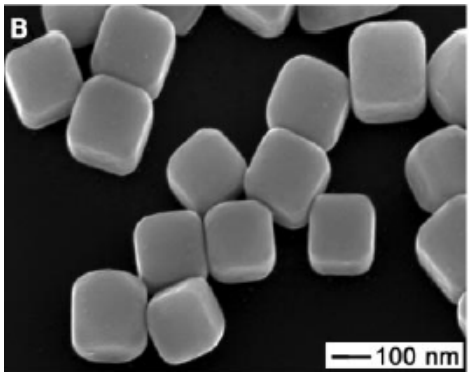

SEM image of Silver Nanocubes[1]

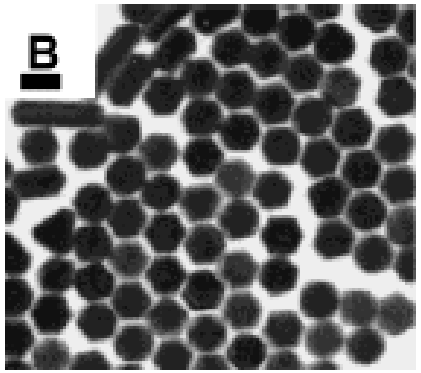

TEM images of Au nanoparticles. Scale 100 nm[2]

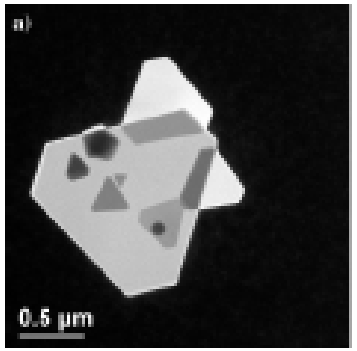

HAADF image of Au nanoparticles: synthesized @ 100°C[3]

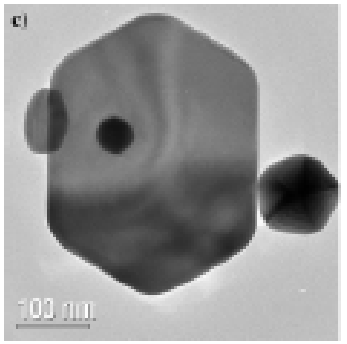

TEM image of particles sinthesized @ 190°C[3]

gold nanorods

Seed-mediated Growth in Solution

1. Chemical reduction of a metal salt with strong reducing agent ($NaBH_4$),
2. Use of a capping agent to prevent particle growth (citrate),
3. Addition of the seeds to a solution that contains more metal salt, a weak reducing agent (AA) and a rodlike micellar template (cetyltrimethylammonium bromide, CTAB).

Aspect ratio is controlled by the ratio of metal seed to metal salt.

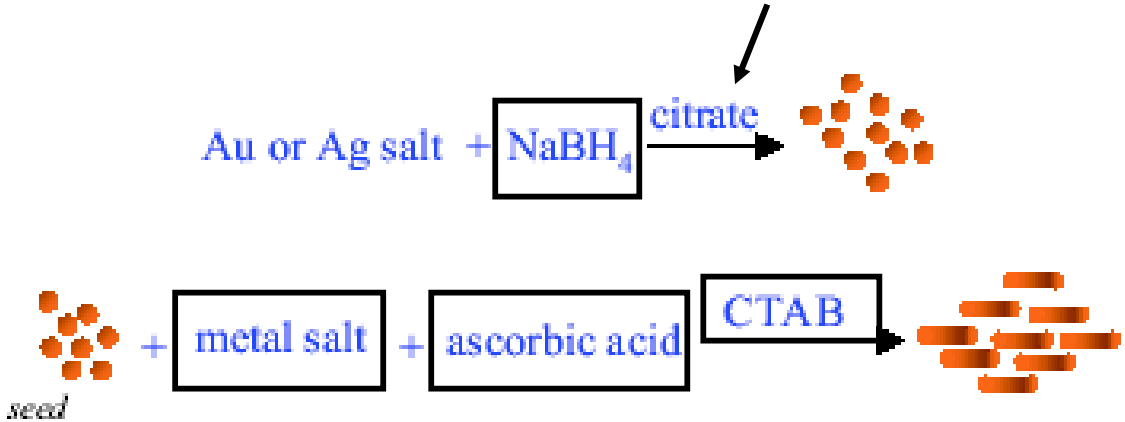

C.J.Murphy, N.R.Jana, Adv.Mater. 2002, 14 (80-82)

gold nanorods

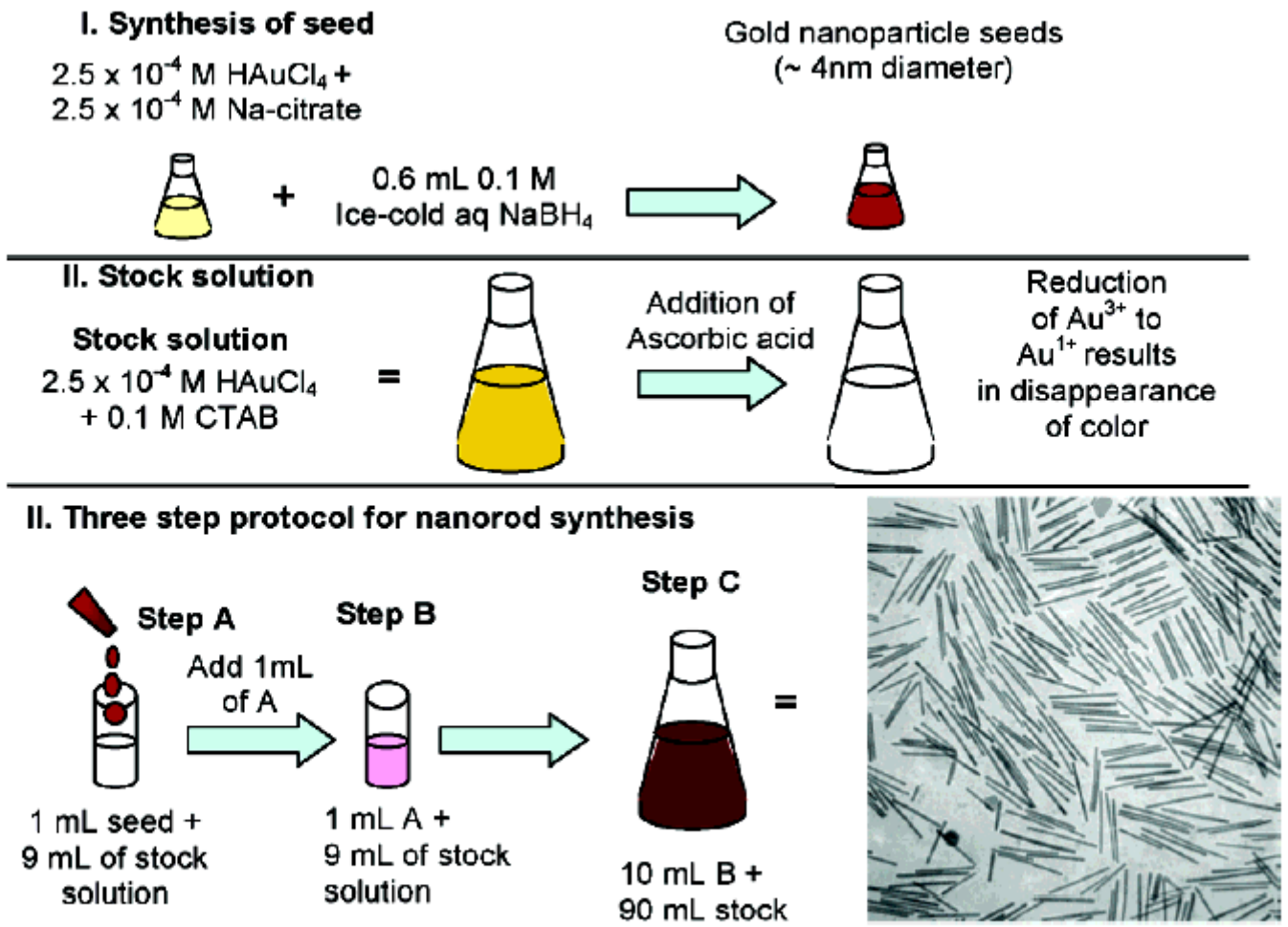

Figure 2. Seed-mediated growth approach to making gold and silver nanorods of controlled aspect ratio. The specific conditions shown here, for 20 mL volume of seed solution, lead to high-aspect ratio gold nanorods. (bottom right) Transmission electron micrograph of gold nanorods that are an average of 500 nm long.

Nikoobahkt and El-Sayed, Chem. Mater. **2003**, 15, 1957;
Sau and Murphy, Langmuir **2004**, 20, 6414.

gold nanorods

Influence of the reaction parameters

✓ Effect of the Seed Concentration

An **increase** in the **$[Au]_{seed}$ decreased** the **rod length** for a given concentration of Au^{3+}.

✓ Effect of AA concentration

The **rod length decreases** with an **increase in [AA]** keeping all other conditions the same.

✓ Effect of $AgNO_3$

When **silver nitrate** is **not used** nanorods are obtained in **low yield** and quite **long**.

✓ Effect of $[Au^{3+}]$

The **less** quantity of **Au^{3+} ions** per seed particle available the **short** are the nanorods.

✓ Effect of [CTAB]

Lower CTAB concentrations can lead to **non-rod-shaped** particles.

gold nanorods

Variation in the absorption of visible light

Short aspect ratio Au nanorods are especially interesting because of their optical properties: they exhibit tranverse and longitudinal plasmon bands.

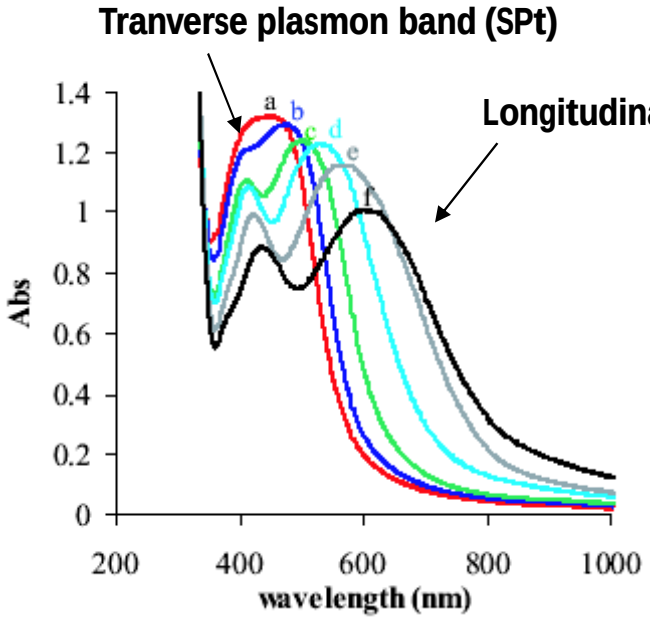

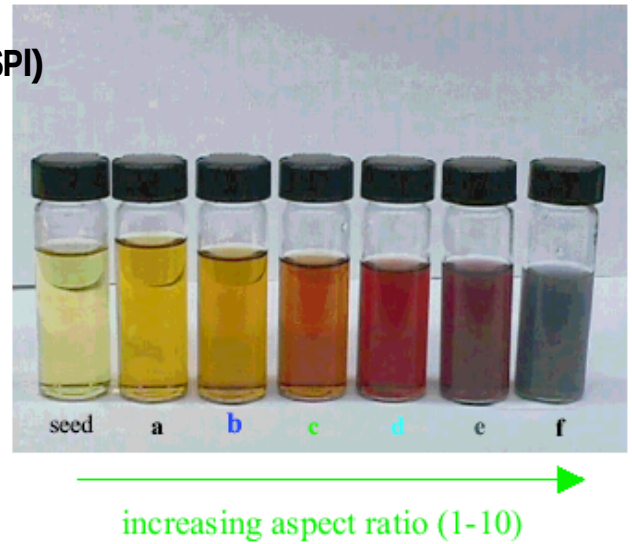

Aspect ratio: the length of the major axis divided by the width of the minor axis.

The larger the aspect ratio, the more red-shifted the longitudinal plasmon band.

gold nanorods

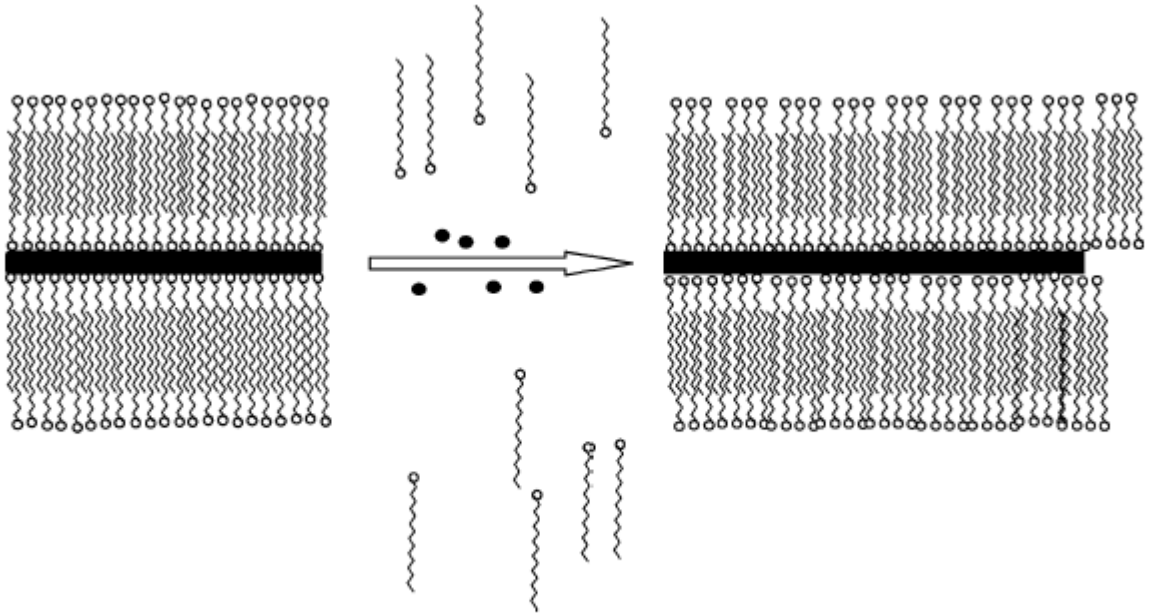

Figure 7. Cartoon illustrating "zipping": the formation of the bilayer of CnTAB (squiggles) on the nanorod (black rectangle) surface may assist nanorod formation as more gold ion (black dots) is introduced. Reproduced from ref 104 with permission.

gold nanorods

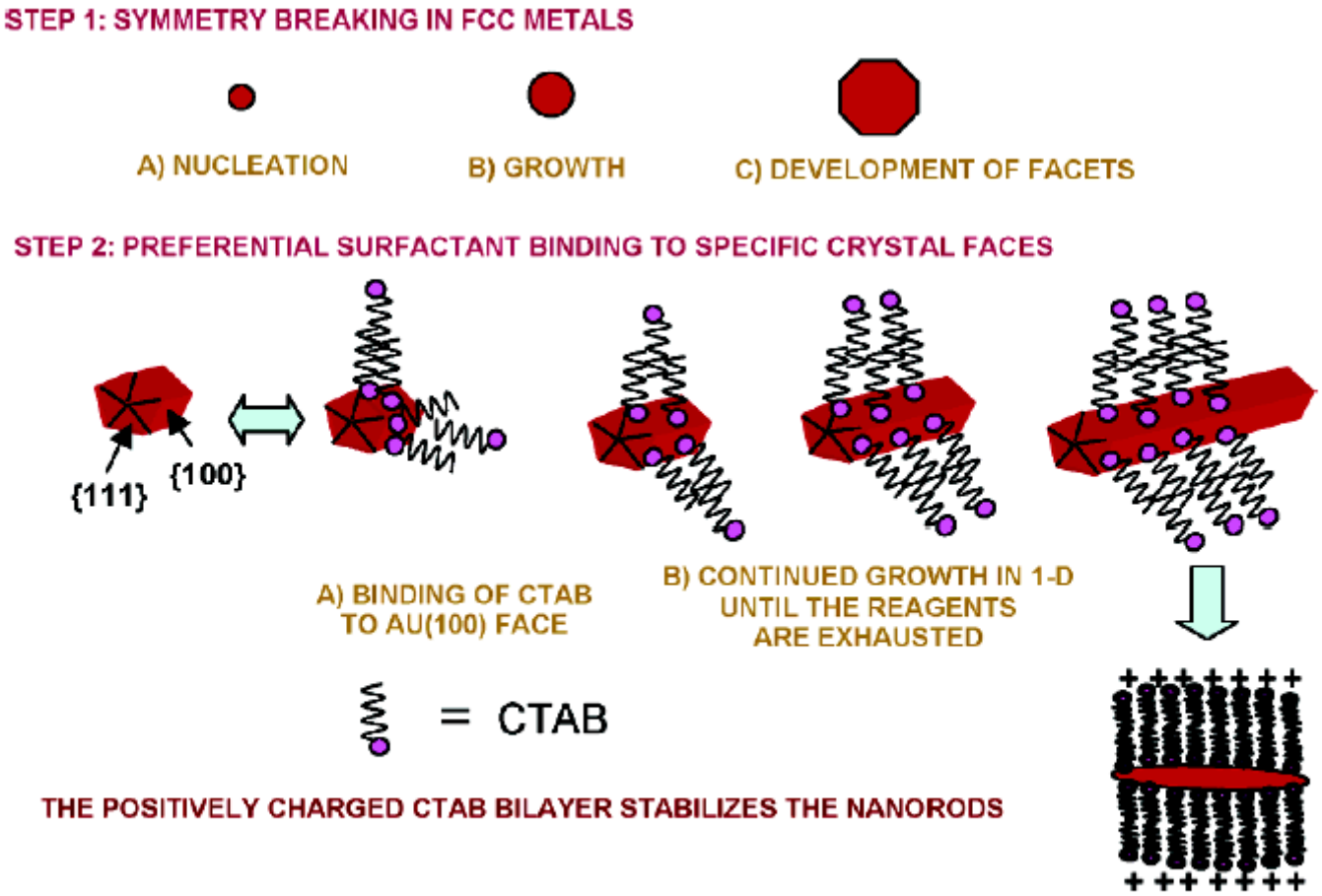

Figure 8. Proposed mechanism of surfactant-directed metal nanorod growth. The single crystalline seed particles have facets that are differentially blocked by surfactant (or an initial halide layer that then electrostatically attracts the cationic surfactant). Subsequent addition of metal ions and weak reducing agent lead to metallic growth at the exposed particle faces. In this example, the pentatetrahedral twin formation leads to Au {111} faces that are on the ends of the nanorods, leaving less stable faces of gold as the side faces, which are bound by the surfactant bilayer.

gold nanorods - functionalization

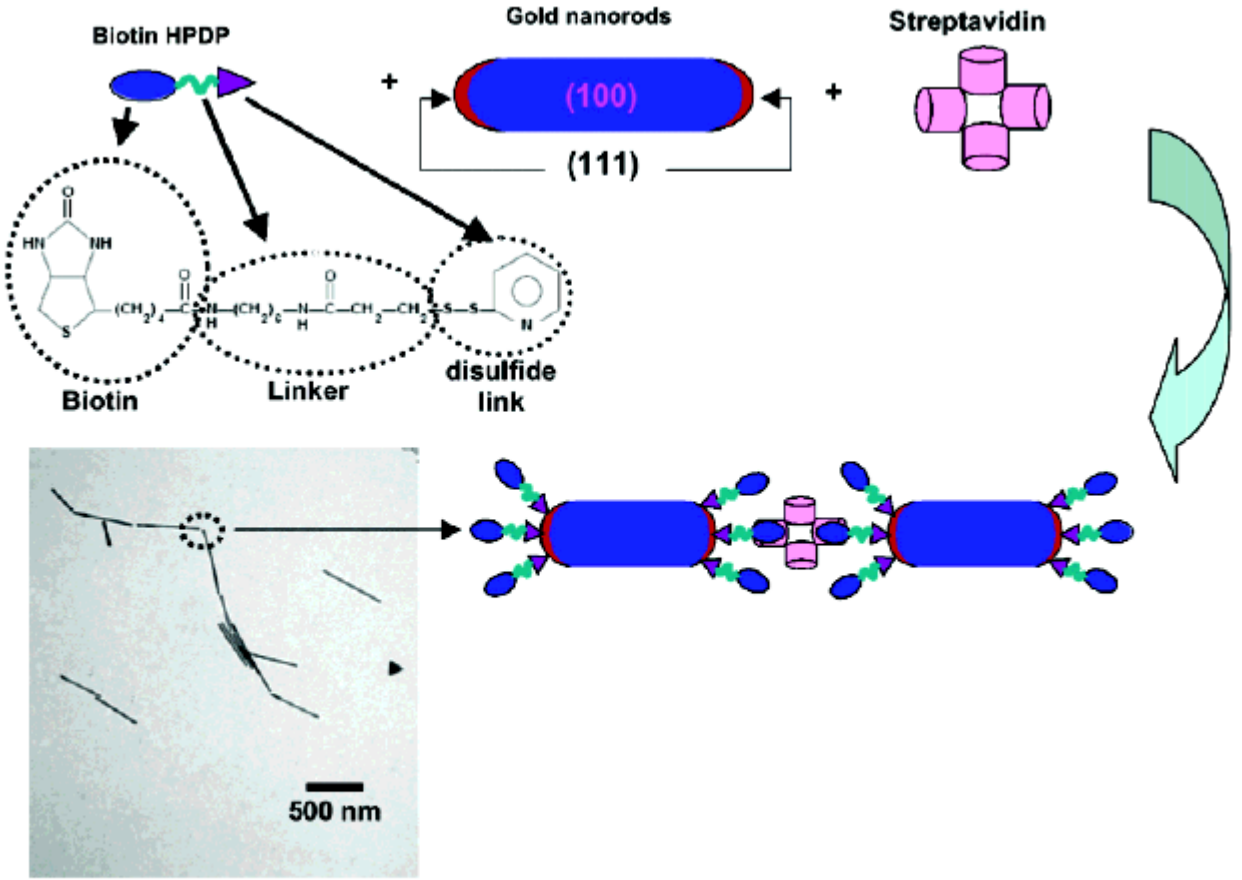

Figure 9. Cartoon of biotin-streptavidin assembly of gold nanorods; a biotin disulfide is added to biotinylate the rods, and subsequent addition of streptavidin causes noncovalent assembly. Inset: transmission electron micrograph of gold nanorod-streptavidin assemblies. The original data are from ref 86.

ANISOTROPIC METAL NANOPARTICLES

Branched structures: Tripods & Tetrapods

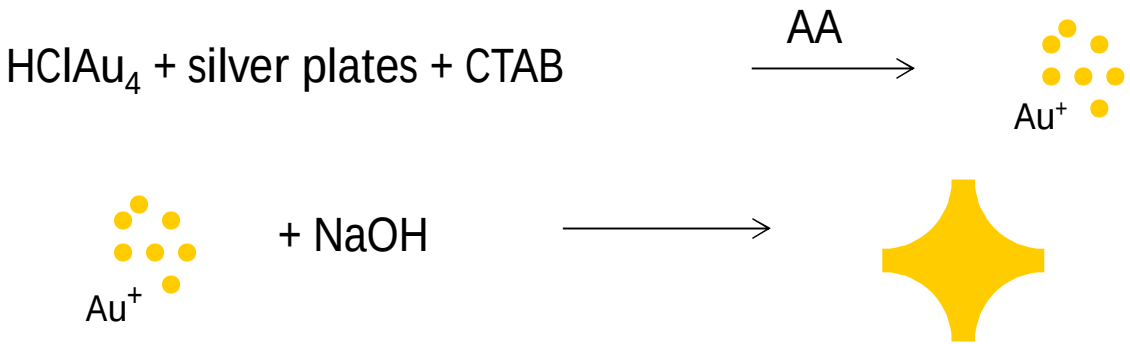

The forced reduction of gold by ascorbic acid through the addition of NaOH is the key step for particle branching.

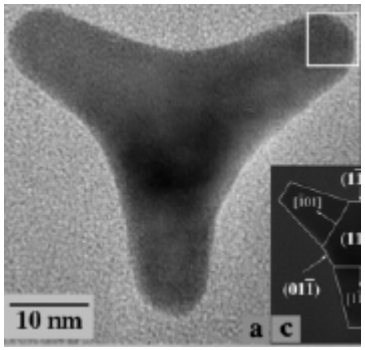

TEM image of a regular tripod nanocrystal

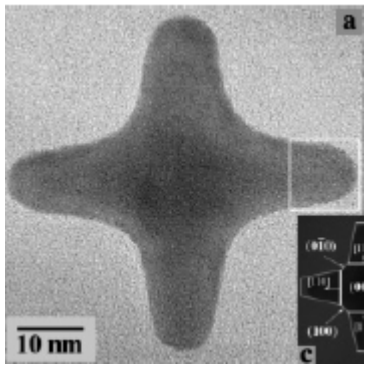

TEM image of a tetrapod nanocrystal

J.Am.Chem.Soc. 2003, 125, 16186-16187

ANISOTROPIC METAL NANOPARTICLES

From Ag nanocubes to Au nanoboxes

When Silver nanocubes are treated with a gold salt, an oxidation-reduction reaction ensues. In this reaction, the silver nanocubes serve as a sacrificial hard template to make hollow crystalline gold nanoboxes.

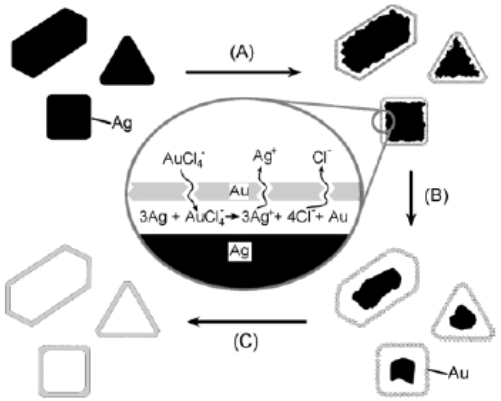

$3\ Ag(s) + HAuCl_4(aq) \longrightarrow Au(s) + 3AgCl(aq) + HCl(aq)$

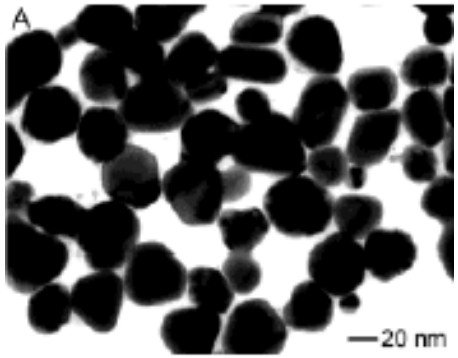

TEM image of silver nanoparticles synthesized using the polyol process.

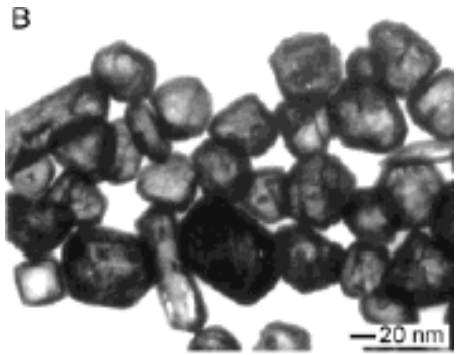

TEM image of gold nanoshells.

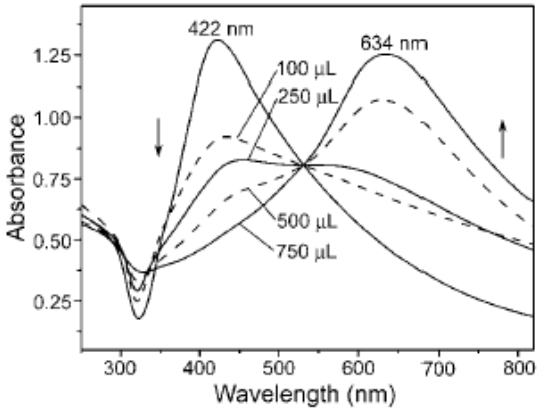

UV-vis absorption spectra of an aqueous dispersion of Ag nanoparticles.

Y. Sun, B.T. Mayers and Y. Xia, Nano Letters, 2, 481- 485

Au nanoboxes

By controlling the molar ratio between Ag and $HAuCl_4$, the gold nanocages could be tuned to display surface plasmon resonance peaks around 800 nm, a wavelength commonly used in optical coherence tomography (OCT) imaging.

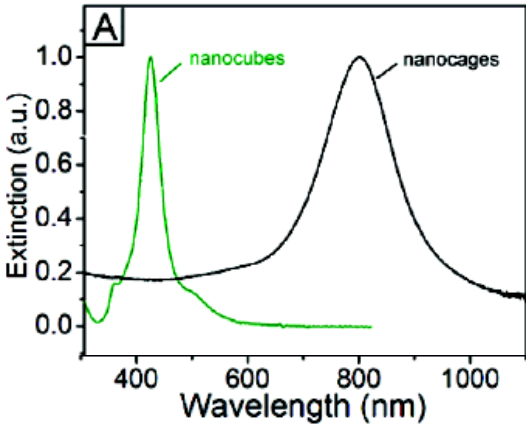

UV exctinction spectra recorded from solutions of Ag nanocubes and Au nanocages.

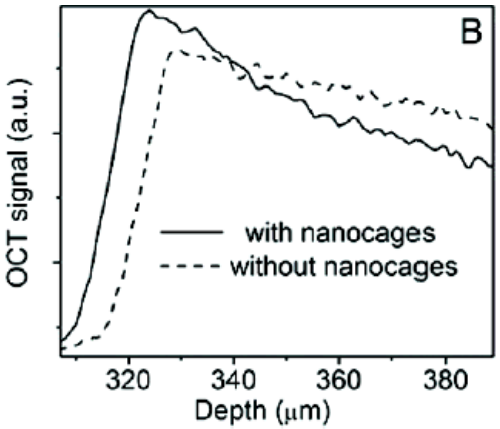

Plot of the OCT signals on a long scale as a function of depth.

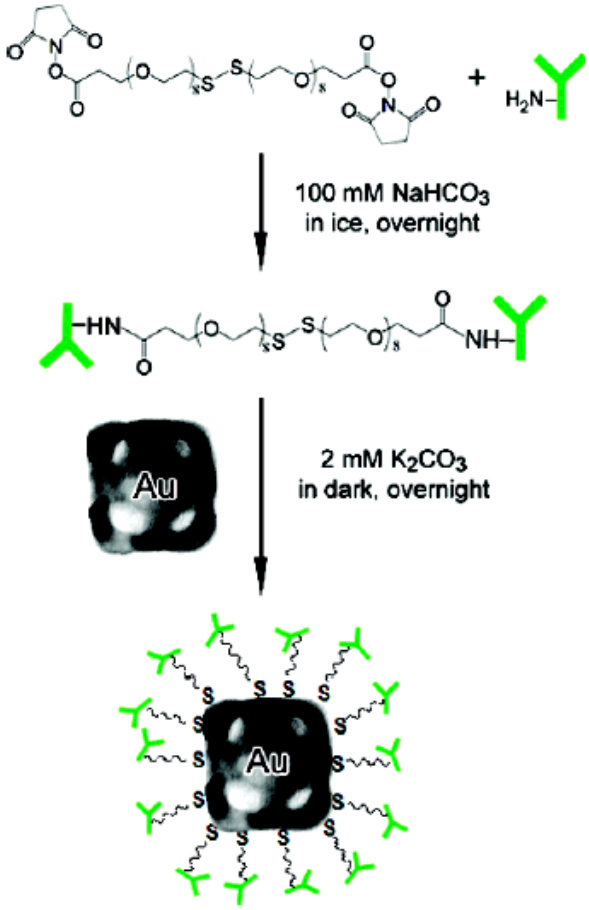

Gold nanocages functionalized with tumor-specific antibodies.

J.Chen, Y.Xia et al, Nano Letters, 2005, 5, 473-477.

Nanoparticles - Applications

- NP for gene and drug delivery
- DNA sensing
- proteins sensing
- recognition and multivalency
- imaging
- enzyme mimiking
- new materials

Nanoparticle-based Sensors

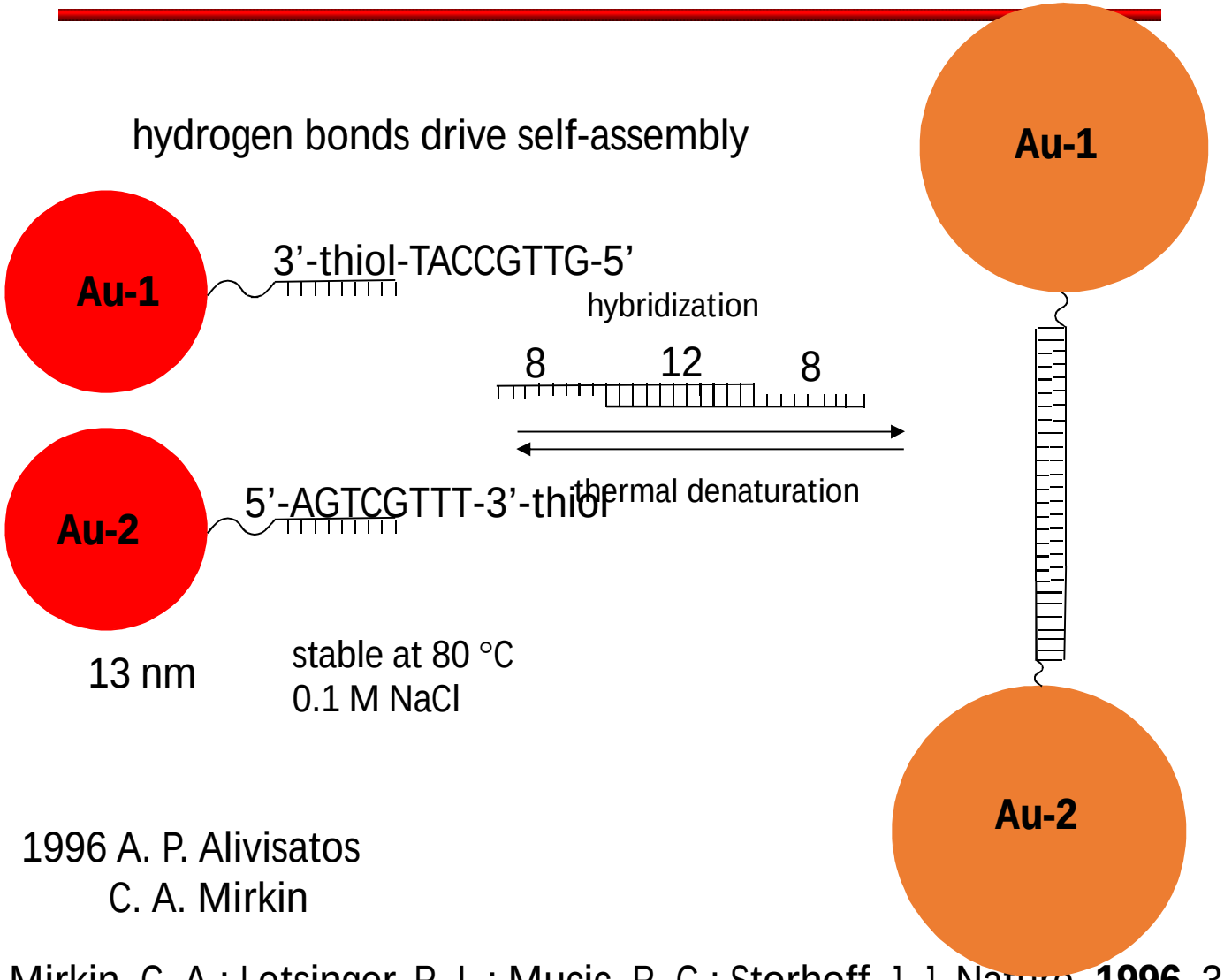

1996 A. P. Alivisatos
C. A. Mirkin

Mirkin, C. A.; Letsinger, R. L.; Mucic, R. C.; Storhoff, J. J. Nature, **1996**, 382, 607-609.
Alivisatos, A. P.; Johnsson, K. P.; Peng, X.; Wilson, T. E.; Loweth, C. J.; Bruchez, M. P. Jr.; Schultz, P. G. Nature, **1996**, 382, 609-611.

Nanoparticle-based Sensors

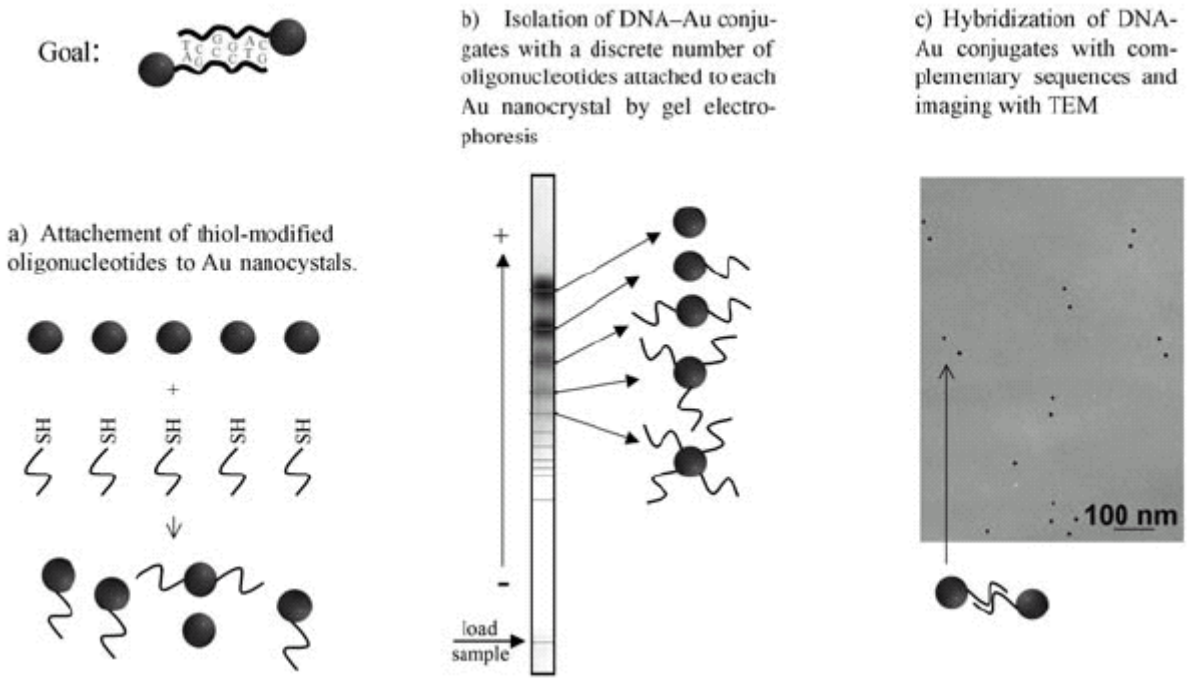

Figure 7. Forming DNA-meditated dimers of Au nanoparticles requires each nanoparticle to be functionalized with one oligonucleotide, with both oligonucleotides being complementary to each other. a) When phosphine- (or citric acid) stabilized Au nanoparticles and thiol-modified oligonucleotides react, DNA binds with its thiol group to the Au surface. However, even for 1:1 mixtures of DNA and Au, Au nanoparticles with more or less than one bound oligonucleotide will result; b) Au nanoparticles with a different number of DNA molecules bound per particle can be sorted by gel electrophoresis (image adapted from ref. [87]). Individual bands of nanoparticles with a discrete number of DNA molecules per particle can be observed and extracted from the gel; c) Au nanoparticles with one DNA molecule can be mixed with another solution of Au nanoparticles modified with a complementary DNA sequence. The single-stranded DNA molecules hybridize to a double strand, thus connecting the Au nanoparticles. The resulting dimers can be observed by TEM imaging (the Au-nanoparticle dimers shown comprise two 10-nm-diameter Au nanocrystals; the DNA molecules cannot be seen by TEM). Image courtesy of D. Zanchet et al.[7]

Alivisatos, A. P.; Johnsson, K. P.; Peng, X.; Wilson, T. E.; Loweth, C. J.; Bruchez, M. P. Jr.; Schu
Nature, **1996**, 382, 609-611.

Nanoparticle-based Sensors

selective colorimetric detection system for polynucleotides

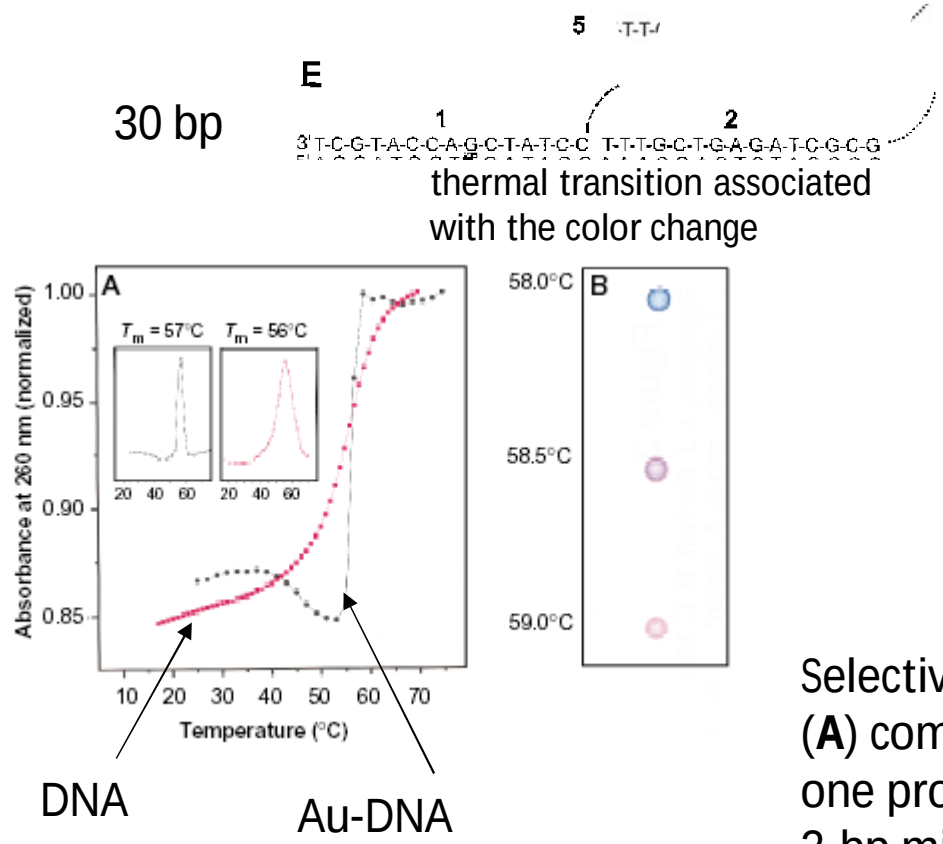

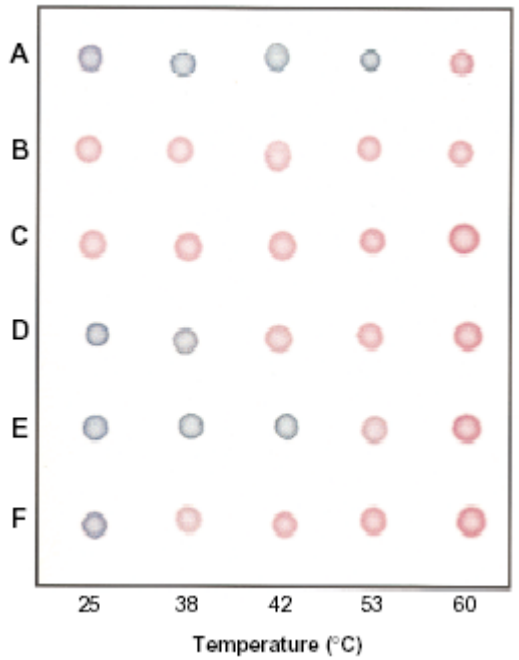

Selective polynucleotide detection for the target pr
(**A**) complementary target; (**B**) no target; (**C**) compl
one probe; (**D**) a 6-bp deletion; (**E**) a 1-bp mismatcl
2-bp mismatch. Nanoparticle aggregates were prep
600-μl thin-walled Eppendorf tube by addition of 1
oligonucleotide target to a mixture containing 50 μ
(0.06 μM final target concentration). The mixture v
in a bath of dry ice and isopropyl alcohol and allow

Elganian, R.; Storhoff, J.J.; Mucic, R. C.; Letsinger, R. L.; Mirkin, C. A. Science **1997**, 277, 1078-1081.

Nanoparticle-based Sensors

selective colorimetric detection system for polynucleotides

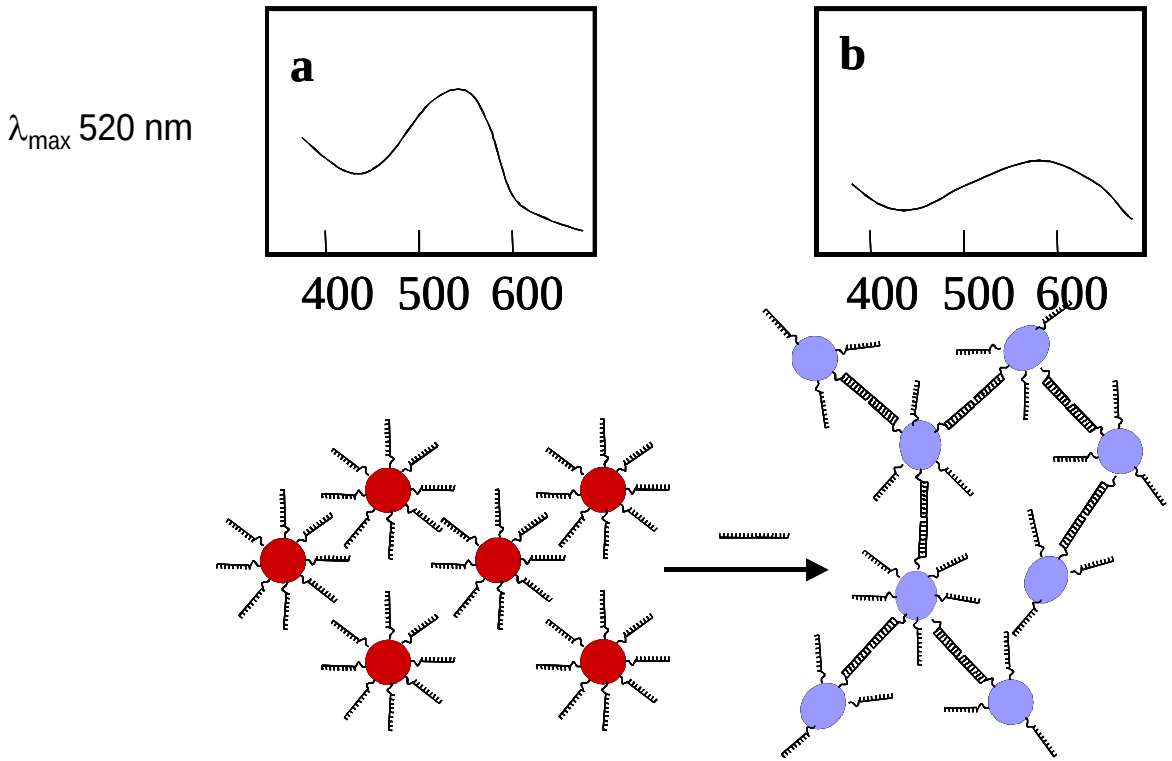

very sensitive: 10 femtomoles of polynucleotide could be detected

Elganian, R.; Storhoff, J.J.; Mucic, R. C.; Letsinger, R. L.; Mirkin, C. A. Science **1997**, 277, 1

Nanoparticle-based Sensors

scanometric DNA array detection

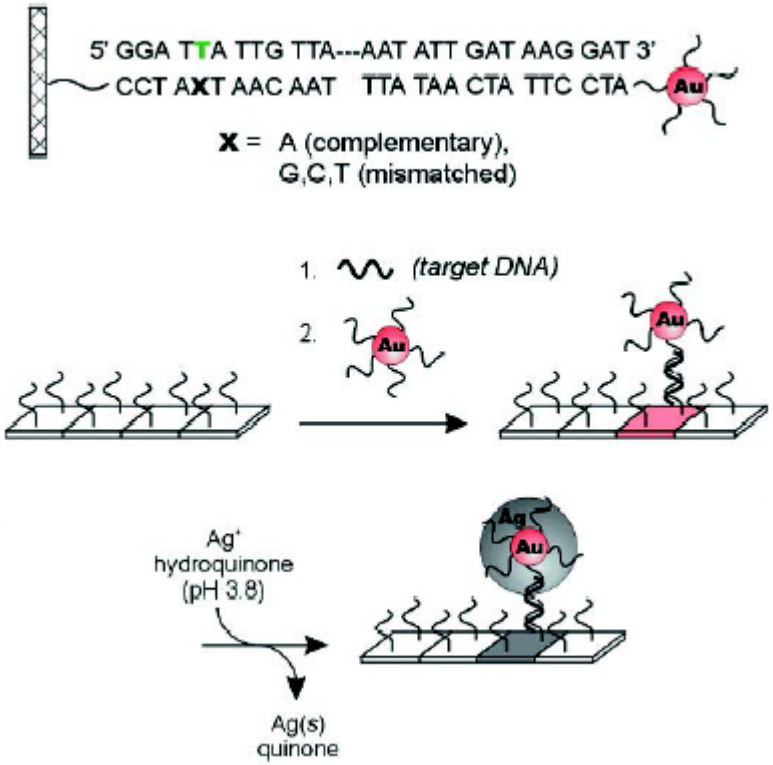

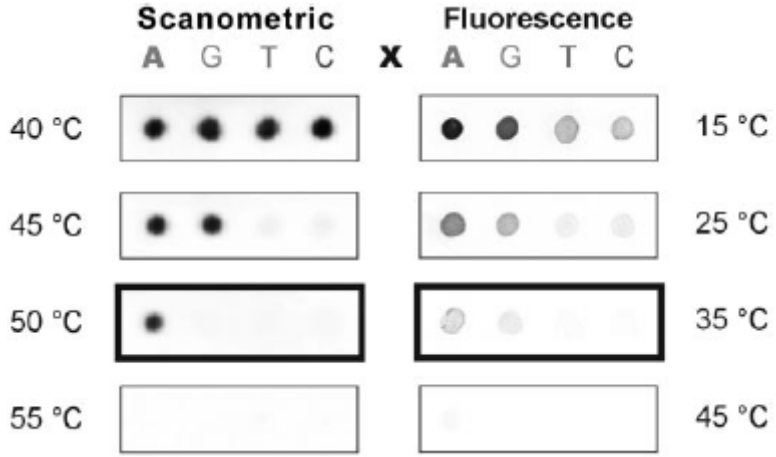

Taton, T. A.; Mirkin, C. A.; Letsinger, R. L. Science **2000**, 289, 1757-1760.

Nanoparticle-based Sensors

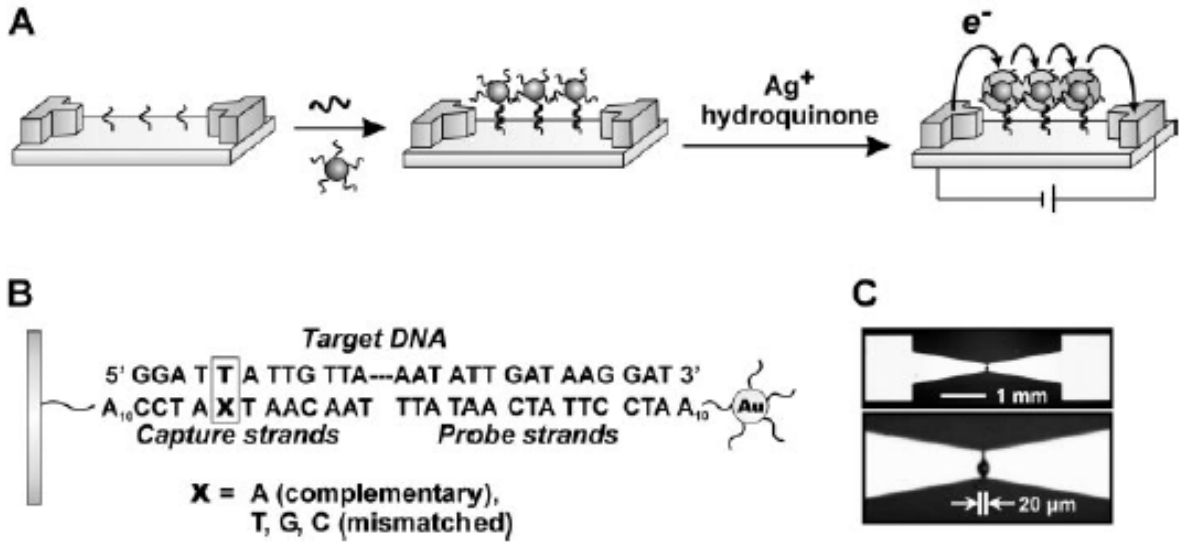

(**A**) Scheme showing concept behind electrical detection of DNA. (**B**) Sequences of capture, target, and probe DNA strands. (**C**) Optical microscope images of the electrodes used in a typical detection experiment. The spot in the electrode gap in the high-magnification image is food dye spotted by a robotic arrayer (GMS 417 Microarrayer, Genetic Microsystems, Woburn, MA).

target DNA was detected at concentrations as low as 500 femtomolar and with a point mutation selectivity factor of ~100,000:1

Park, S. J.; Taton, T. A.; Mirkin, C. A. Science **2002**, 295, 1503-1506.

Gold nanoparticles-based protease assay

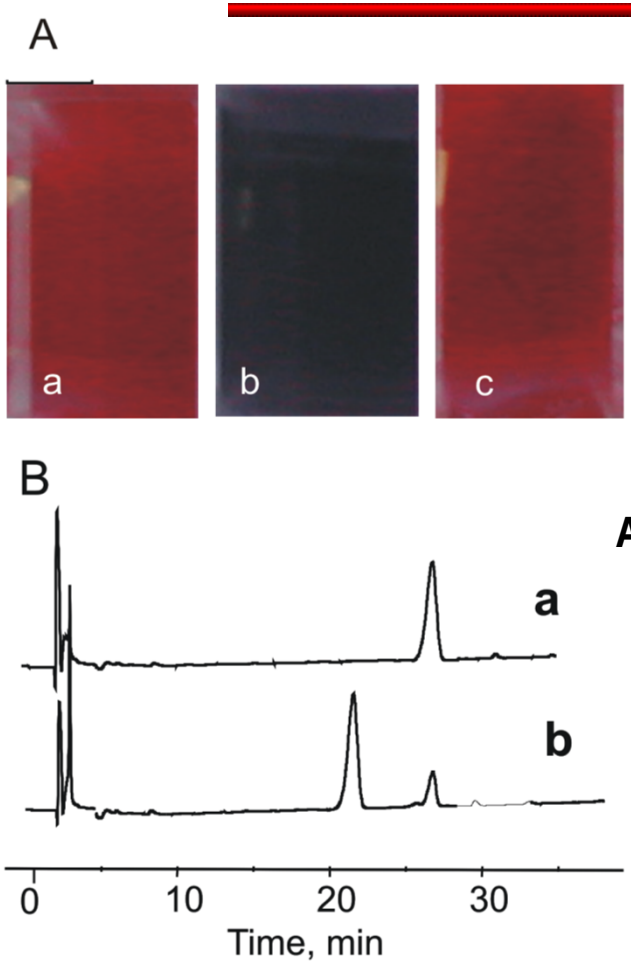

Ac-Cys(S-Ac)-Gly-DPhe-Pro-LArg-Gly-Cys(S-Ac)-OH, 1.

Ac-Cys(S-Ac)-Leu-Arg-Arg-Arg-Arg-Val-Tyr-Pro-Tyr-Pro- nor-Leu-Glu-Leu-Cys(S-Ac)-OH, 2.

Figure 1. A. Color of the gold colloids: (a) untreated solution; (b) 5 min after the additio
(c) 5 min after the addition of **1** ([**1**]final=62 nM) incubated for 90 min with thrombin ([t
B. RP-HPLC chromatogram of the original peptide **1** (upper trace, a) and after exposition
(lower trace, b). Conditions: [**1**]final=62 μM, [thrombin]= 30 nM, pH=8, 25°C. The peak a
to the fragment Ac-Cys(S-Ac)-Gly-(D)Phe-Pro-Arg-OH.

C. Guarise, L. Pasquato, V. De Filippis, P. Scrimin, Proc. Natl. Acad. Sci. U.S.A., **2006**, 103, 397

Gold nanoparticles-based protease assay

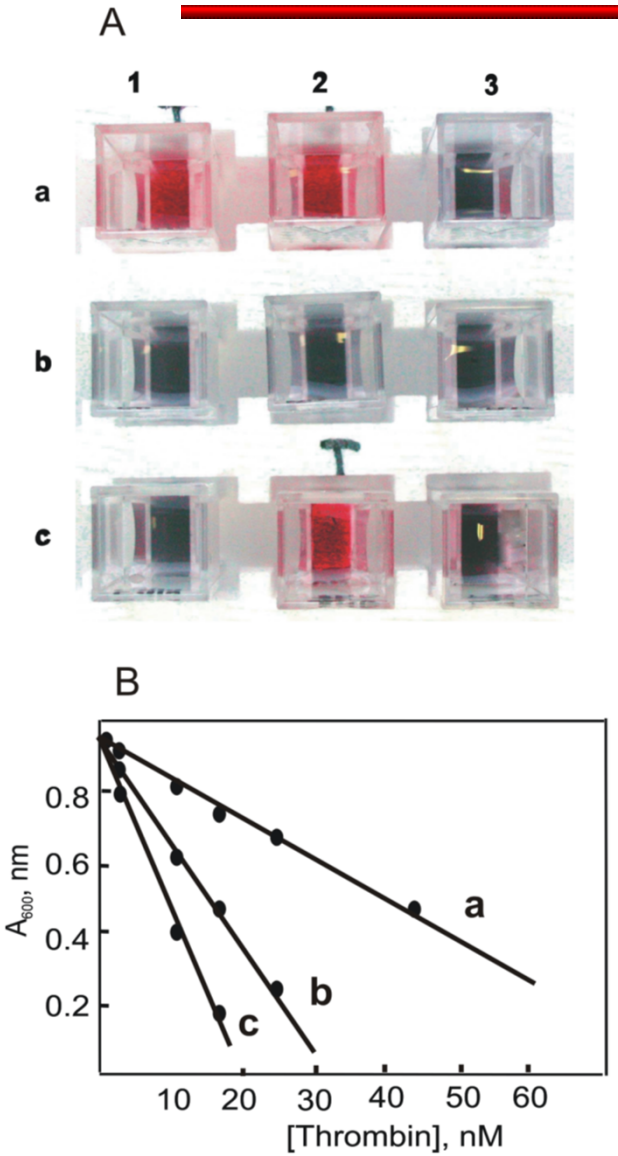

Fig. 3. Thrombin assay. (A) Colorimetric test for the presen
Each cuvette contained the following enzymes: a1, chymot
factor Xa, and thrombin; a2, chymotrypsin and thrombin; a
plasmin, and factor Xa; b1, factor Xa and chymotrypsin; b2
factor Xa; c1, none; c2, thrombin; c3, plasmin. (B) Absorba
gold colloid solution after addition of a solution of peptide
exposed to different concentrations of thrombin for 30 mi
(line b), and 90 min (line c) at pH 8 and 25°C.

C. Guarise, L. Pasquato, V. De Filippis, P. Scrimin, Proc. Natl. Acad. Sci. U.S.A., **2006**, 103,

Gold nanoparticles-based protease assay

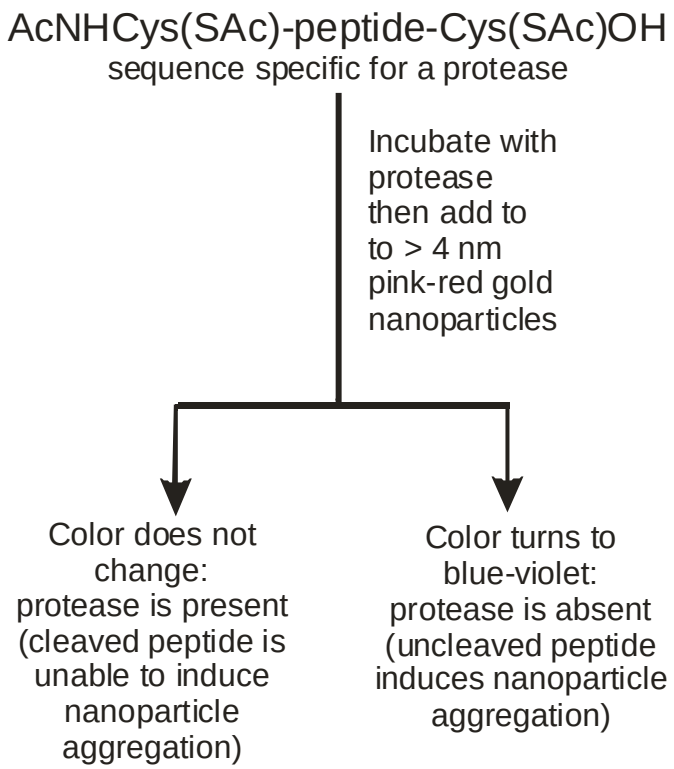

C. Guarise, L. Pasquato, V. De Filippis, P. Scrimin, Proc. Natl. Acad. Sci. U.S.A., **2006**, 103, 3978-

Hybrid Nanoparticle−Liposome Detection of Phospholipase Activity

Daniel Aili†, Morgan Mager†, David Roche and Molly M. Stevens
Nano Letters 2010

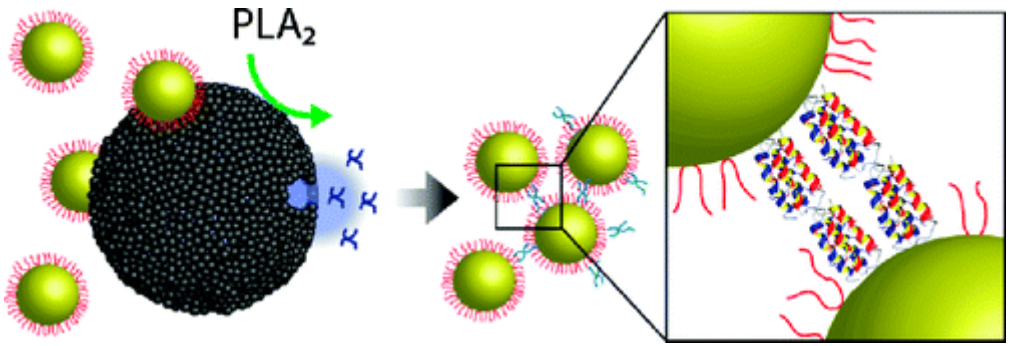

A flexible nanoparticle-based phospholipase (PL) assay is demonstrated in which the enzymatic substrate is decoupled from the nanoparticle surface. Liposomes are loaded with a polypeptide that is designed to heteroassociate with a second polypeptide immobilized on gold nanoparticles. Release of this polypeptide from the liposomes, triggered by PL, induces a folding-dependent nanoparticle bridging aggregation. The colorimetric response from this aggregation enables straightforward and continuous detection of PL in the picomolar range. The speed, specificity, and flexibility of this assay make it appropriate for a range of applications, from point of care diagnostics to high-throughput pharmaceutical screening.

A nanoplasmonic molecular ruler for measuring nuclease activity and DNA footprinting

G. L. LIU, Y. YIN, S. KUNCHAKARRA, B. MUKHERJEE, D. GERION,
S. D. JETT, D. G. BEAR, J. W. GRAY, A. P. ALIVISATOS, L. P. LEE1, F. F.CHEN
nature nanotechnology **2006**, 1, 47

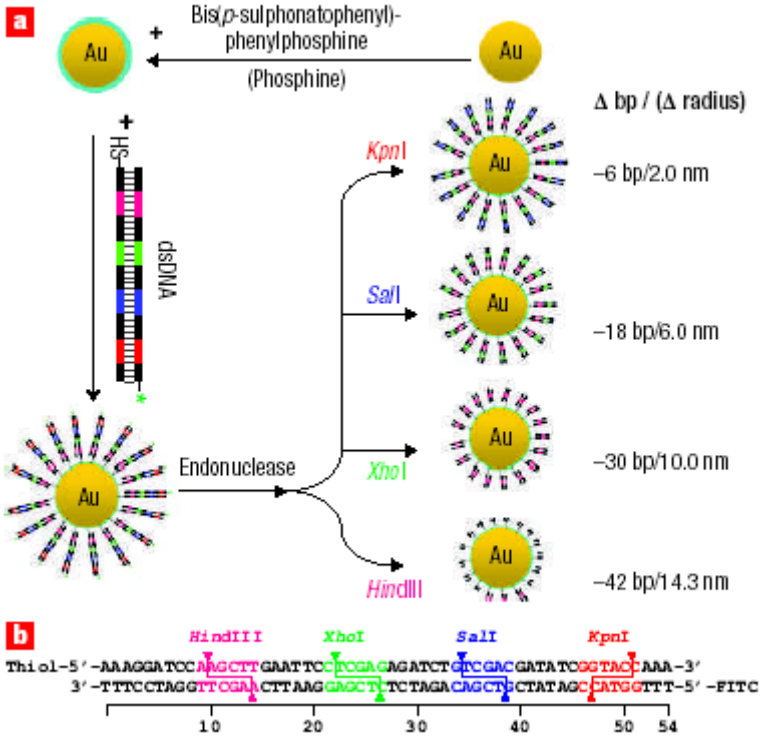

Figure 1. Design of the Au–DNA nanoplasmonic molecular ruler. a, Synthesis process of the Au–DNA nanoconjugate. The 20-nm Au nanoparticle modified with a phosphine surfactant monolayer was enclosed by a layer of synthesized 54-bp dsDNA. A thiol group and the FITC (fluorescein isothiocyanate) fluorophore (as indicated by green star) were synthesized at each end of the dsDNA, respectively. Through the thiol–Au chemistry, the dsDNA was tethered onto the Au nanoparticles. b, The dsDNA contains endonuclease incision sites

catalytic activity of MPC-C12-TEG-C12-P2-H

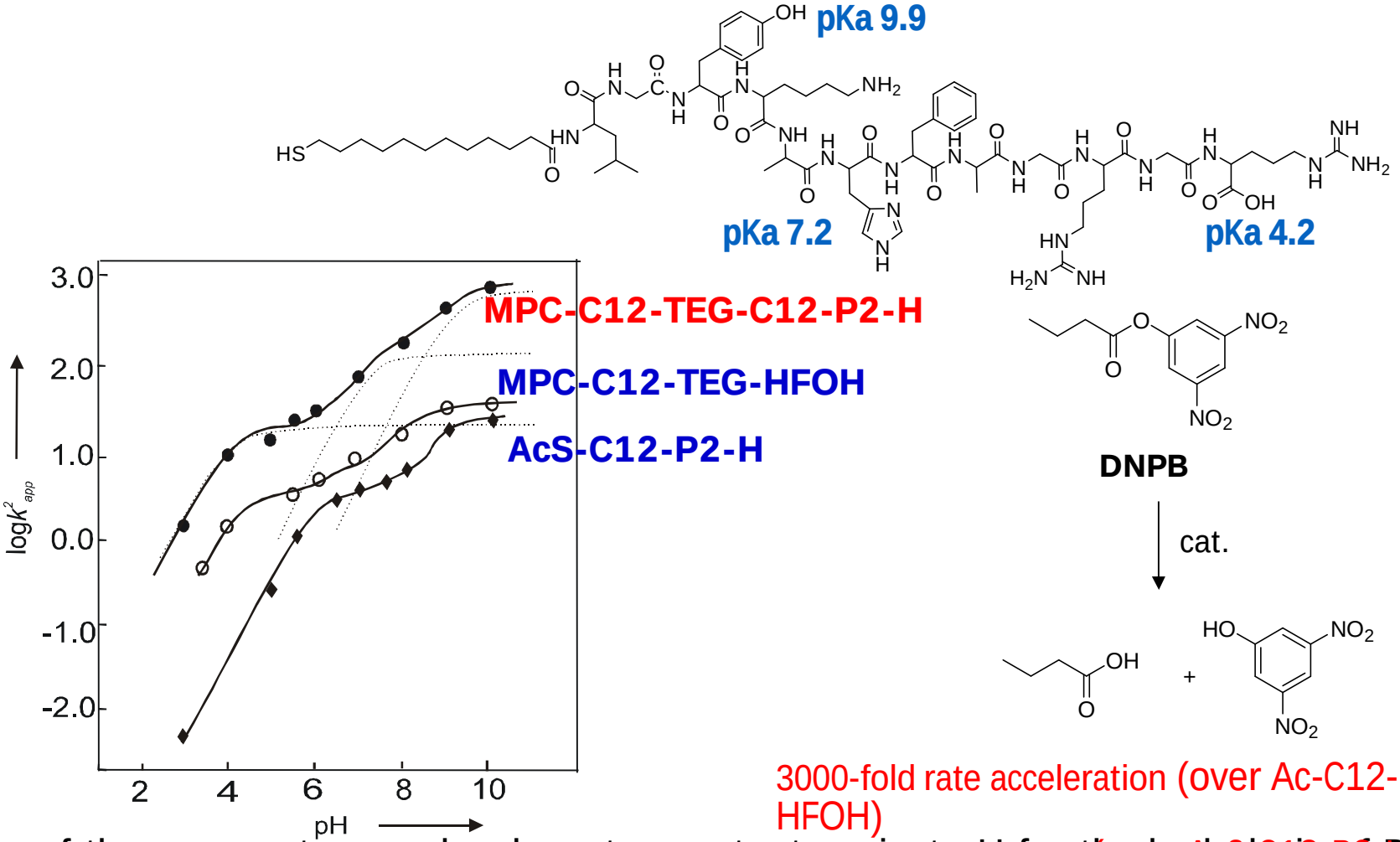

Log of the apparent second order rate constant against pH for the hydrolysis of DNPB c
Au-PEP (●) nanoparticles Au-**2** (○), and S-acetylated peptide **1** (♦). The solid lines repr
the dissociation of residues involved in catalysis with pKa values of 4.2, 7.2 and 9.9, in
and 6.1 and 9.2 for S-acetylated **1**. The dotted lines represent the calculated contributi
Au-PEP. Conditions: [catalyst]=4.0×10^{-5} M, [buffer]=10-20 mM, 25°C.

Pengo, P.; Baltzer, L.; Pasquato, L.; Scrimin, P. Angew. Chem. Int. Ed. **2007**

catalytic activity of MPC-C8-TEG-C12-P2-H

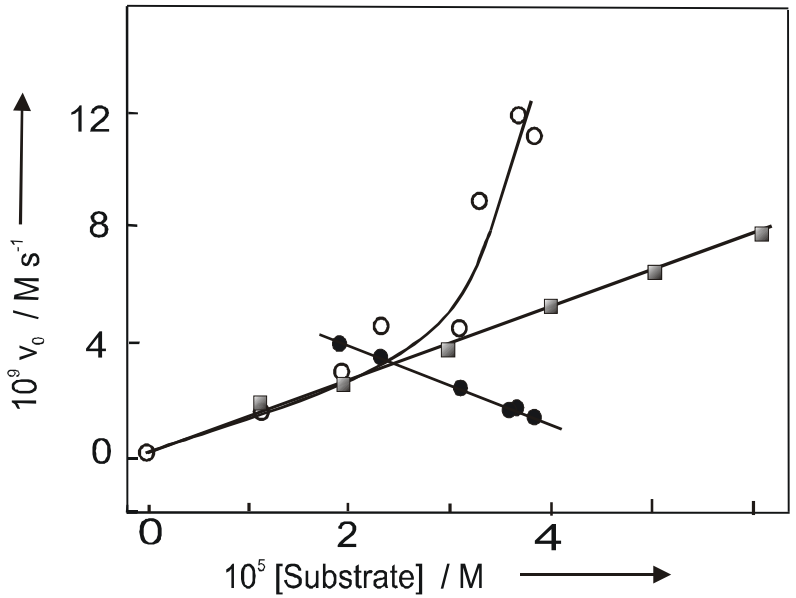

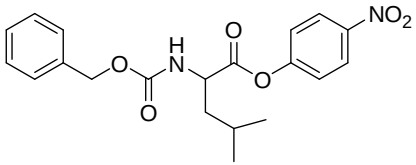

Z-(L)-Leu-ONp

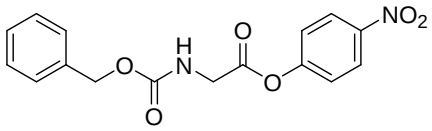

Z-Gly-ONp

DNPB behaves as Z-Gly-ONp

Figure 2. Dependence of the initial rate (M s^{-1}) of intermediate formation (○) and it and that of hydrolysis (■) with Z-Gly-PNP upon substrate concentration. Conditions: (bound to Au-PEP), pH 7, 25°C.

$$\text{Cat} + \text{S} \underset{k_-}{\overset{k_+}{\rightleftharpoons}} \text{Cat-S} \xrightarrow{k_{cat}} \text{Cat-S'} + \text{P1} \xrightarrow{k_2} \text{Cat} + \text{P2}$$

serine-proteases like

Pengo, P.; Baltzer, L.; Pasquato, L.; Scrimin, P. Angew. Chem. Int. Ed. **2007**, 46

Detection and identification of proteins using nanoparticle–fluorescent polymer ‘chemical nose’ sensors

C.-C. YOU, O. R. MIRANDA, B. GIDER1, P. S. GHOSH, I.-B. KIM,
B. ERDOGAN1, S. A. KROVI, U. H. F. BUNZ, VINCENT M. ROTELLO

nature nanotechnology VOL 2 | MAY 2007 , page 318

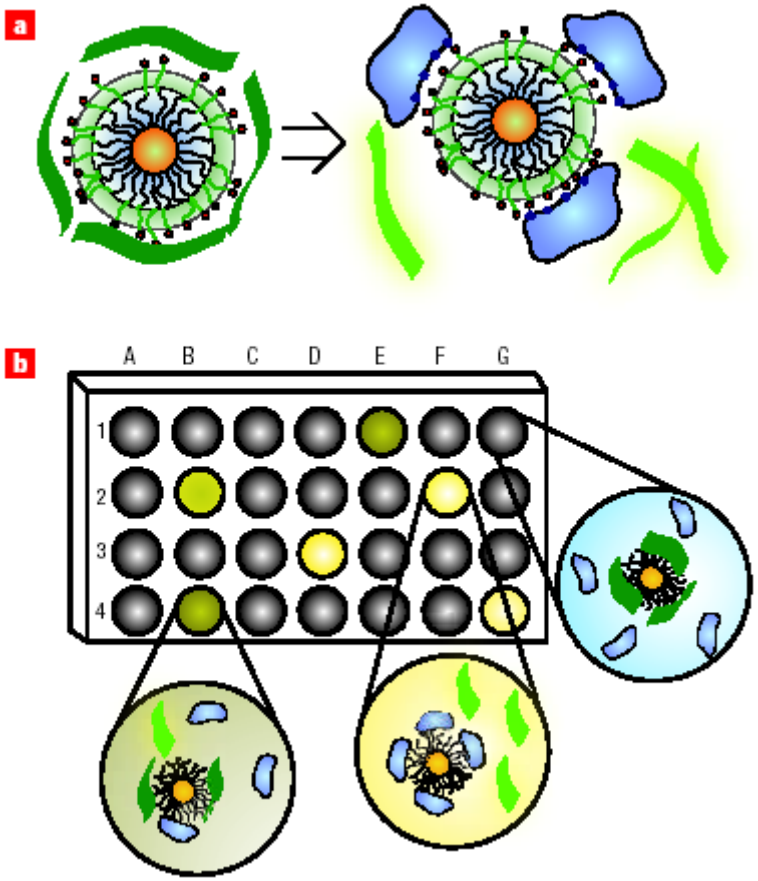

Figure 1 Fluorophore displacement protein sensor array. a, Displacement of quenched fluorescent polymer (dark green strips, fluorescence off; light green strips, fluorescence on) by protein analyte (in blue) with concomitant restoration of fluorescence. The particle monolayers feature a hydrophobic core for stability, an oligo(ethylene glycol) layer for biocompatibility, and surface charged residues for interaction with proteins. **b**, Fluorescence pattern generation through differential release of fluorescent polymers from gold nanoparticles. The wells on the microplate contain different nanoparticle–polymer conjugates, and the addition of protein analytes produces a fingerprint for a given protein.

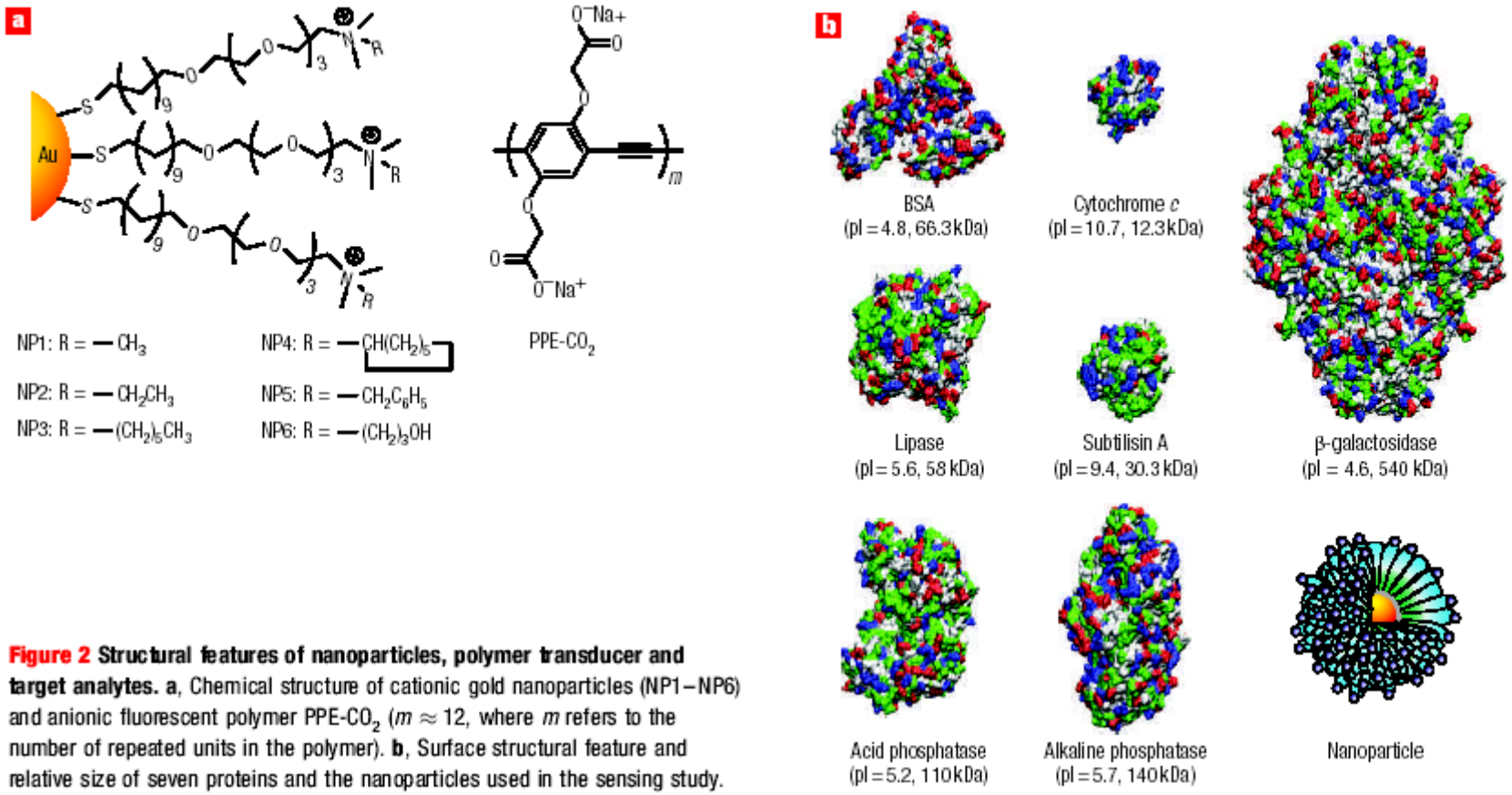

Figure 2 Structural features of nanoparticles, polymer transducer and target analytes. a, Chemical structure of cationic gold nanoparticles (NP1–NP6) and anionic fluorescent polymer PPE-CO_2 ($m \approx 12$, where m refers to the number of repeated units in the polymer). **b**, Surface structural feature and relative size of seven proteins and the nanoparticles used in the sensing study. Colour scheme for the proteins: nonpolar residues (grey), basic residues (blue), acidic residues (red) and polar residues (green).

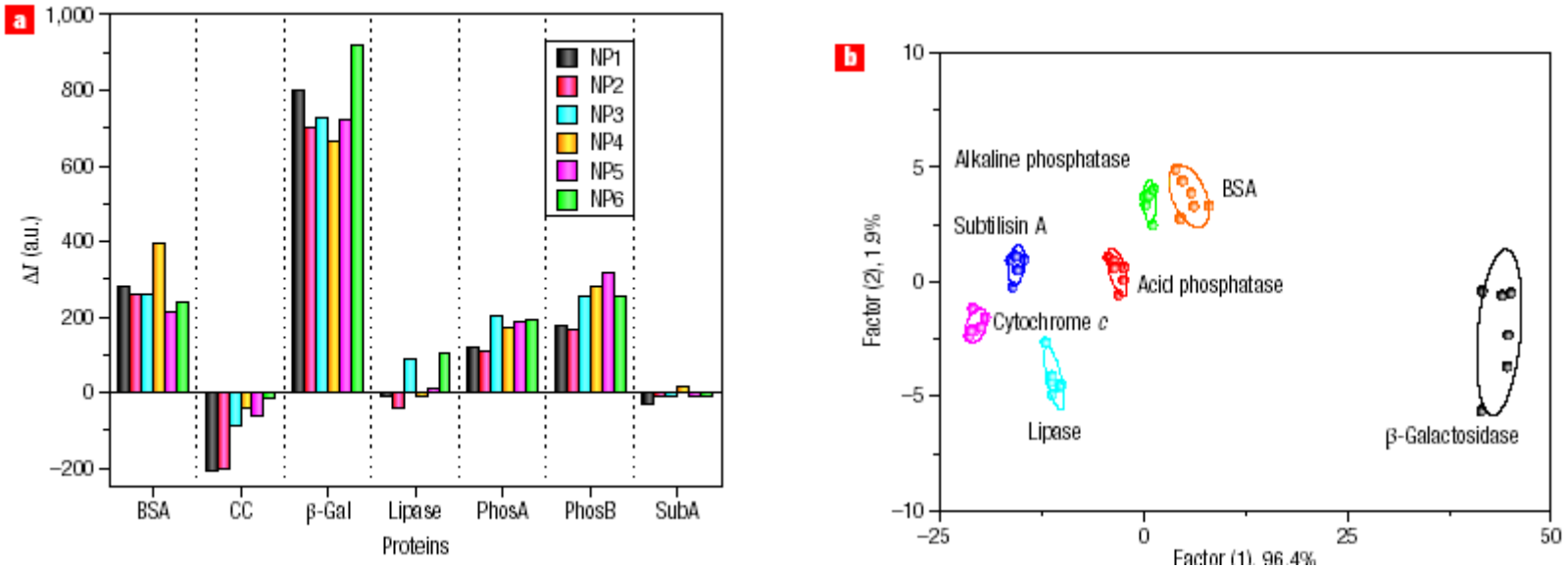

Figure 4 Array-based sensing of protein analytes at 5 μM. a, Fluorescence response (ΔI) patterns of the NP–PPE sensor array (NP1–NP6) against various proteins (CC, cytochrome *c*; β-Gal, β-galactosidase; PhosA, acid phosphatase; PhosB, alkaline phosphatase; SubA, subtilisin A). Each value is an average of six parallel measurements. **b**, Canonical score plot for the first two factors of simplified fluorescence response patterns obtained with NP–PPE assembly arrays against 5 μM proteins. The canonical scores were calculated by LDA for the identification of seven proteins. The 95% confidence ellipses for the individual proteins are also shown.

LDA = linear discriminant analysis

photothermal therapy

travel as far through living tissue as a magnetic field can. "We wanted something that

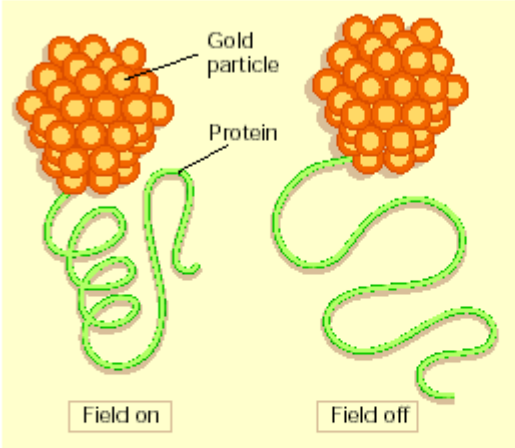

Kimberly Hamad-Schifferli (right) hopes to control proteins by attaching tiny gold particles to them — in a radio field the particle heats up, altering the protein's structure and inactivating it.

'nano' word is over-used and over-hyped," says John Ryan, director of the Nanobiotech-

paced activities of daily life in the cell. And for those in the nanosystems alliance, nanotechnology is the best way to get a grip on the many fleeting processes involved. Alliance member Leroy Hood, a molecular biologist at the Institute for Systems Biology in Seattle, predicts that nanotechnology will reveal as much new information about the cell as did the automated DNA sequencer — a device that he invented. "The combination of microfluidics and nanotechnology," Hood asserts, "will transform how biologists do everything." ■

Catherine Zandonella is a freelance writer in New York.

1. Melosh, N. A. *et al. Science* **300**, 112–115 (2003).
2. Vo-Dinh, T. *J. Cell. Biochem.* **87**, 154–161 (2002).
3. Klarreich, E. *Nature* **413**, 450–452 (2001).
4. Quintana, A. *et al. Pharm. Res.* **19**, 1310–1316 (2002).
5. Hamad-Schifferli, K., Schwartz, J. J., Santos, A. T., Zhang, S. & Jacobson J. M. *Nature* **415**, 152–155 (2002).

Alliance for NanoSystems Biology

www.nanosysbio.org